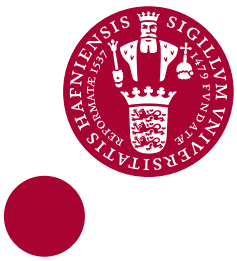

Obesity-Associated Hypermetabolism and Accelerated Senescence of Bone Marrow Stromal Stem Cells Suggest a Potential Mechanism for Bone Fragility

Tencerova, Michaela; Frost, Morten; Figeac, Florence; Nielsen, Tina Kamilla; Ali, Dalia; Lauterlein, Jens Jacob Lindegaard; Andersen, Thomas Levin; Haakonsson, Anders Kristian; Rauch, Alexander; Madsen, Jonna Skov; Ejersted, Charlotte; Højlund, Kurt; Kassem, Moustapha

Published in:
Cell Reports

DOI:
10.1016/j.celrep.2019.04.066

Publication date:
2019

Document version
Publisher's PDF, also known as Version of record

Article

Cell Reports

Obesity-Associated Hypermetabolism and Accelerated Senescence of Bone Marrow Stromal Stem Cells Suggest a Potential Mechanism for Bone Fragility

Graphical Abstract

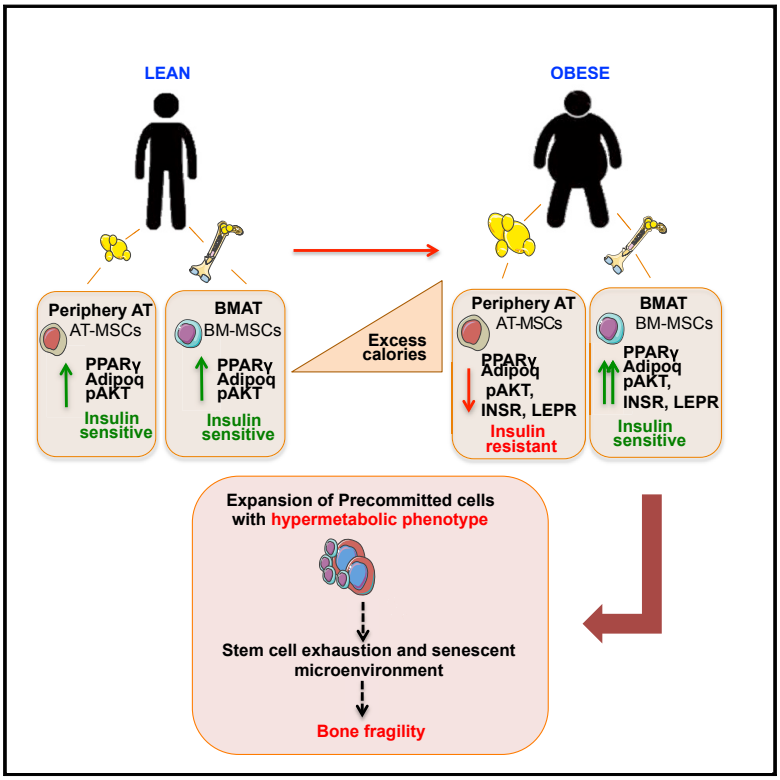

Highlights

- Obesity accelerates differentiation potential of bone marrow stromal stem cells (BM-MSCs)
- Obesity shifts molecular phenotype of BM-MSCs toward committed adipocytic progenitors
- Obesity increases insulin signaling in BM-MSCs in contrast to adipose tissue-derived MSCs
- IR+ and LEPR+ cells in obese BM-MSCs are associated with accelerated senescence

Authors

Michaela Tencerova, Morten Frost, Florence Figeac, ..., Charlotte Ejersted, Kurt Højlund, Moustapha Kassem

Correspondence

mtencerova@health.sdu.dk

In Brief

Tencerova et al. show that in human obesity, BM-MSCs exhibit a hypermetabolic state defined by upregulation of insulin signaling with enhanced adipogenesis and increased intracellular reactive oxygen species (ROS), leading to a senescence bone microenvironment contributing to bone fragility. Moreover, increased abundance of IR+ and LEPR+ BM-MSCs is characteristic of this phenotype, with an activated metabolic rate in obese subjects.

Tencerova et al., 2019, Cell Reports *27*, 2050–2062
May 14, 2019
https://doi.org/10.1016/j.celrep.2019.04.066

CellPress

OPEN ACCESS
CellPress

Cell Reports
Article

Obesity-Associated Hypermetabolism and Accelerated Senescence of Bone Marrow Stromal Stem Cells Suggest a Potential Mechanism for Bone Fragility

Michaela Tencerova,[1,6,11,*] Morten Frost,[1,2] Florence Figeac,[1] Tina Kamilla Nielsen,[1] Dalia Ali,[1] Jens-Jacob Lindegaard Lauterlein,[1] Thomas Levin Andersen,[3,4,5] Anders Kristian Haakonsson,[1,6] Alexander Rauch,[1] Jonna Skov Madsen,[7,8] Charlotte Ejersted,[9] Kurt Højlund,[2,4] and Moustapha Kassem[1,10]

[1]Department of Molecular Endocrinology, KMEB, University of Southern Denmark and Odense University Hospital, 5000 Odense C, Denmark
[2]Steno Diabetes Center Odense, Odense University Hospital, 5000 Odense C, Denmark
[3]Clinical Cell Biology, Department of Pathology, Odense University Hospital, 5000 Odense C, Denmark
[4]Department of Clinical Research, University of Southern Denmark, 5000 Odense C, Denmark
[5]Department of Molecular Medicine, University of Southern Denmark, 5000 Odense C, Denmark
[6]OPEN, Odense Patient Data Explorative Network, Odense University Hospital, Odense, Denmark
[7]Institute of Regional Health Science, University of Southern Denmark, 5000 Odense C, Denmark
[8]Department of Biochemistry and Immunology, Lillebaelt Hospital, 7100 Vejle, Denmark
[9]Department of Endocrinology, Odense University Hospital, 5000 Odense C, Denmark
[10]Department of Cellular and Molecular Medicine, DanStem (Danish Stem Cell Center), Panum Institute, University of Copenhagen, Copenhagen, Denmark
[11]Lead Contact
*Correspondence: mtencerova@health.sdu.dk
https://doi.org/10.1016/j.celrep.2019.04.066

SUMMARY

Obesity is associated with increased risk for fragility fractures. However, the cellular mechanisms are unknown. Using a translational approach combining RNA sequencing and cellular analyses, we investigated bone marrow stromal stem cells (BM-MSCs) of 54 men divided into lean, overweight, and obese groups on the basis of BMI. Compared with BM-MSCs obtained from lean, obese BM-MSCs exhibited a shift of molecular phenotype toward committed adipocytic progenitors and increased expression of metabolic genes involved in glycolytic and oxidoreductase activity. Interestingly, compared with paired samples of peripheral adipose tissue-derived stromal cells (AT-MSCs), insulin signaling of obese BM-MSCs was enhanced and accompanied by increased abundance of insulin receptor positive (IR+) and leptin receptor positive (LEPR+) cells in BM-MSC cultures. Their hyper-activated metabolic state was accompanied by an accelerated senescence phenotype. Our data provide a plausible explanation for the bone fragility in obesity caused by enhanced insulin signaling leading to accelerated metabolic senescence of BM-MSCs.

INTRODUCTION

Obesity is a major health problem worldwide, and besides metabolic complications such as insulin resistance, type 2 diabetes (T2D), and liver steatosis, bone fragility is increasingly recognized (Napoli et al., 2017). Recent epidemiological studies have reported an association between obesity and increased risk for fragility fractures at several anatomical sites (Gonnelli et al., 2014). This is paradoxical because obesity is associated with normal or increased bone mass and is traditionally thought to be protective against fragility fractures because of higher bone mass caused by increased mechanical loading on the skeleton and higher estrogen levels (Wardlaw, 1996). Obesity is associated with increased bone marrow adipose tissue (BMAT) that alters bone marrow (BM) composition and thus may change bone architecture and bone material properties that contribute to reduced bone quality (Ambrosi et al., 2017; Boskey and Imbert, 2017; Naveiras et al., 2009; Rubin et al., 2007). However, the cellular mechanisms underlying these changes are not known.

BMAT originates from BM stromal (also known as skeletal or mesenchymal) stem cells (BM-MSCs), which also give rise to osteoblastic bone-forming cells (Gimble et al., 2006). The differentiation potential of BM-MSCs is tightly regulated via several factors present in the BM microenvironment, including secreted proteins and hormones (Tencerova and Kassem, 2016). Some of these factors (e.g., secreted frizzled-related protein [sFRP-1] and legumain [LGMN]) determine the commitment of BM-MSCs into the adipocyte or osteoblast lineages (Abdallah and Kassem, 2012; Jafari et al., 2017). Under steady-state conditions, there is a balance between BM-MSCs and their committed progenitors. However, this balance alters with aging and osteoporosis because of microenvironmental changes (Kassem and Marie, 2011).

Similar to aging, the BM microenvironment undergoes significant metabolic changes in obesity. Previous studies have reported increased BMAT and changes in immune cell differentiation and level of inflammation (Adler et al., 2014; Bredella et al.,

Table 1. Clinical and Biochemical Characteristics of Study Participants

Clinical and Biochemical Data	Lean (n = 19)	Overweight (n = 15)	Obese (n = 20)
Age (years)	31 ± 3	32 ± 3	37 ± 2[a]
Weight (kg)	75.2 ± 1.8	95.4 ± 2.7[b]	117.2 ± 3.2[c]
Height (cm)	181.0 ± 1.1	184.1 ± 1.9	179.9 ± 1.3
BMI (kg/m^2)	22.9 ± 0.3	28.0 ± 0.4[b]	36.1 ± 0.8[c]
Waist (cm)	83.0 ± 1.2	100.0 ± 2.7[b]	118.9 ± 2.6[c]
Hip (cm)	95.1 ± 0.9	106.1 ± 1.6[b]	113.9 ± 1.2[c]
WHR	0.87 ± 0.01	0.94 ± 0.02[d]	1.04 ± 0.02[c]
Fasting glucose (mmol/L)	5.2 ± 0.1	5.4 ± 0.1	5.8 ± 0.1[c]
Fat free mass (kg)	63.3 ± 1.2	72.0 ± 2.0[b]	76.0 ± 1.6[c]
Fat mass (kg)	11.9 ± 0.8	23.4 ± 1.2[b]	41.2 ± 2.1[c]
Android/gynoid fat ratio	0.40 ± 0.02	0.46 ± 0.04[e]	0.73 ± 0.06[c]
HDL cholesterol (mmol/L)	1.18 ± 0.04	1.11 ± 0.08	1.01 ± 0.04[f]
LDL cholesterol (mmol/L)	2.66 ± 0.15	3.07 ± 0.25	3.00 ± 0.11[a]
Total cholesterol (mmol/L)	4.29 ± 0.17	4.75 ± 0.28	4.77 ± 0.16[a]
Triglycerides (mmol/L)	1.00 ± 0.10	1.24 ± 0.17	1.81 ± 0.33[a]
PTH (pmol/L)	3.5 ± 0.3	3.8 ± 0.5	3.9 ± 0.4
25-hydroxy vitamin D (nmol/L)	62.4 ± 5.2	57.9 ± 6.0	50.0 ± 4.2
Leukocytes (10^9/L)	5.6 ± 0.3	5.8 ± 0.3	6.7 ± 0.4[a]

HDL, high-density lipoprotein; LDL, low-density lipoprotein; PTH, parathyroid hormone; WHR, waist-to-hip ratio.
[a]$p < 0.05$, lean versus obese (two-tailed unpaired Student's t test).
[b]$p < 0.001$, lean versus overweight.
[c]$p < 0.001$, lean versus obese (two-tailed unpaired Student's t test).
[d]$p < 0.01$, lean versus overweight.
[e]$p < 0.05$, lean versus overweight.
[f]$p < 0.01$, lean versus obese (two-tailed unpaired Student's t test).

2011; Doucette et al., 2015; Tencerova et al., 2018). Obesity is also associated with hyperinsulinemia. Insulin signaling is a nutrient-sensing pathway regulating whole-body energy metabolism but is also associated with a senescence phenotype in different tissues (Anisimov, 2003; LaFever and Drummond-Barbosa, 2005). Depletion of insulin receptor (IR) in adipose tissue (AT) protects from obesity-induced insulin resistance and increases lifespan in mice (Blüher et al., 2003). In the present study, we hypothesized that obesity induces an accelerated senescence phenotype in the BM microenvironment and results in changes in the cellular composition of BM-MSCs.

Disease states lead to tissue dysfunction through changes in cellular composition. The effects of obesity on the cellular composition of BM and BM-MSCs have not been studied. Recent lineage-tracing studies have identified a number of BM-MSC lineage markers (Ambrosi et al., 2017; Chan et al., 2015; Post et al., 2008; Zhou et al., 2014). Zhou et al. (2014) identified leptin receptor (LEPR) as a marker of adult murine BM-MSCs. LEPR signaling promotes adipogenesis in mouse BM-MSCs (Yue et al., 2016). In human BM-MSCs, LEPR expression is upregulated with aging (Laschober et al., 2009). Furthermore, IR is another cell surface marker determining self-renewal and regulation of differentiation potential of the stem cells (Xia et al., 2015), as demonstrated in peripheral AT-derived stromal cells (AT-MSCs) and hematopoietic, intestinal, and neuronal stem cells (Andres et al., 2013; Blüher et al., 2002; Cinti et al., 1998; Xia et al., 2015; Ziegler et al., 2015), but its role in BM-MSCs has not been studied.

Thus, we examined in a case-control study the presence of intrinsic changes in cellular, molecular, and metabolic characteristics as well as senescence phenotype of BM-MSCs in obese subjects.

RESULTS AND DISCUSSION

Obesity-Associated Increase in Bone Mass Is Accompanied by Low Bone Turnover

To investigate whether obesity affects the cellular and molecular phenotype of BM-MSCs, we enrolled 54 healthy men subdivided into groups of lean, overweight (OW), and obese on the basis of BMI. Obesity-related anthropometric parameters (weight, BMI, and waist circumference) were significantly different among the groups (Table 1). Body composition measured using dual-energy x-ray absorptiometry (DXA) scanning showed increased android/gynoid ratio with increasing BMI, suggesting visceral fat accumulation (Table 1). Basal biochemical parameters revealed higher levels of fasting glucose, insulin, low-density lipoprotein (LDL) cholesterol, triglyceride, and leukocyte count in obese compared with lean subjects. Moreover, insulin resistance status, as assessed by homeostasis model assessment of IR (HOMA-IR), was significantly different among groups, with higher values observed with increased BMI (Table S1). Other fasting and oral glucose tolerance test (OGTT)-based indices of insulin sensitivity and insulin secretion showed reduced insulin sensitivity and a compensatory increase in insulin secretion with increasing BMI (Table S1). Thus, obese subjects were in a pre-diabetic condition along with a state of a low-grade inflammation demonstrated by increased circulating levels of pro-inflammatory markers and reduced adiponectin (Table S2), corroborating previous findings (Klimcáková et al., 2011).

We observed differences in bone mass among the groups. DXA scanning showed significantly increase in total hip bone mineral density (BMD) but no detectable differences in lumbar spine (L1–L4) BMD in obese compared with lean subjects (Table 2). In addition, serum biochemical markers of bone turnover were decreased with increasing BMI (Table 2), and P1NP/CTx was increased in obese patients (Table 2), suggesting decreased bone turnover, similar to what has previously been reported in obese persons, denoting the absence of selection bias (Tonks et al., 2017). The molecular mechanism responsible for increased bone mass and low turnover in obesity is not clear, but a number of hypotheses have been proposed, including higher levels of insulin, lower levels of IGF-1, and changes in BM-MSC differentiation (Hayden et al., 1995; Napoli et al., 2017; Tonks et al., 2017). The presence of higher levels of pro-inflammatory markers is

Table 2. Bone Mass Measurements of DXA Scan of Hip and Spine and Serum Levels of Bone Turnover Markers

	Lean (n = 19)	Overweight (n = 15)	Obese (n = 20)
DXA Scan Data: Hip			
Trochanter area (cm^2)	13.2 ± 0.2	13.4 ± 0.6	13.4 ± 0.4
BMC trochanter (g)	9.7 ± 0.4	10.1 ± 0.6	10.7 ± 0.4 (p = 0.08)
BMD trochanter (g/cm^2)	0.735 ± 0.025	0.750 ± 0.022	0.800 ± 0.025 (p = 0.07)
Intertrochanteric area (cm^2)	24.4 ± 0.7	26.3 ± 1.0	23.6 ± 0.5
BMC intertrochanteric (g)	28.8 ± 1.0	31.3 ± 1.7	30.4 ± 0.8
BMD intertrochanteric (g/cm^2)	1.19 ± 0.03	1.19 ± 0.03	1.30 ± 0.03[a]
Neck area (cm^2)	5.8 ± 0.1	6.0 ± 0.1	5.8 ± 0.1
BMC neck (g)	5.08 ± 0.19	5.20 ± 0.24	5.33 ± 0.15
BMD neck (g/cm^2)	0.88 ± 0.03	0.87 ± 0.03	0.92 ± 0.03
Total hip area (cm^2)	43.4 ± 0.8	45.7 ± 1.4	42.8 ± 0.7
BMC total hip (g)	43.6 ± 1.4	46.6 ± 2.4	46.4 ± 1.2
BMD total hip (g/cm^2)	1.01 ± 0.03	1.02 ± 0.03	1.09 ± 0.03[a]
DXA Scan Data: Spine			
BMD L1–L4 (g/cm^2)	1.02 ± 0.03	1.04 ± 0.03	1.07 ± 0.02
Bone Turnover Markers			
P1NP (μg/L)	85.9 ± 5.9	67.7 ± 5.8[b]	61.9 ± 4.5[c]
CTX1 (ng/L)	0.75 ± 0.1	0.59 ± 0.1	0.44 ± 0.03[d]
P1NP/CTX1	121.5 ± 5.4	113.2 ± 4.8	145.2 ± 7.6[a]
Trap5b (U/L)	4.6 ± 0.4	3.5 ± 0.3[b]	2.7 ± 0.2[d]

BMC, bone mineral content; BMD, bone mineral density; CTX1, C-telopeptide of type I collagen; P1NP, procollagen type I amino-terminal propeptide; Trap5b, tartrate-resistant acid phosphatase 5b.
[a]$p < 0.05$, lean versus obese (two-tailed unpaired Student's t test).
[b]$p < 0.05$, lean versus overweight.
[c]$p < 0.01$, lean versus obese (two-tailed unpaired Student's t test).
[d]$p < 0.001$, lean versus obese (two-tailed unpaired Student's t test).

usually associated with increased bone turnover, thus the presence of a low bone turnover state suggests that BM microenvironment is protected from obesity-associated inflammation. Previous animal studies have demonstrated the absence of high-fat diet (HFD)-induced inflammation in BM and endothelial cell dysfunction causing BM microangiopathy and creating a BM barrier from the peripheral milieu (Mangialardi et al., 2013; Oikawa et al., 2010; Shadduck et al., 1989; Tencerova et al., 2018).

Obesity Is Associated with Distinct Changes in Metabolic Programming of BM-MSCs

To further study cell autonomous changes associated with obesity, we performed RNA sequencing (RNA-seq) of BM-MSCs isolated from lean and obese individuals. We identified 129 genes upregulated and 168 genes downregulated significantly in BM-MSCs of obese compared with lean subjects (Figure 1A; Figure S1A; Table S3). In order to elucidate the functionality of the differentially expressed genes, we performed Gene Ontology (GO) enrichment analyses. Genes that exhibited higher expression in obese BM-MSCs are annotated as genes of fat cell differentiation, osteoblast differentiation, extracellular matrix organization, and immune system processes, while genes associated with glucose metabolic processes and response to hypoxia were downregulated in obese subjects (Figure 1B; Figure S1B). Interestingly, the gene expression signature of obese BM-MSCs suggests an increased presence of committed BM-MSC progenitors and decreased stemness.

Because GO analysis highlighted glucose metabolism to be affected in obese BM-MSCs, we further examined the expression of a number of metabolic processes genes. We observed increased expression of genes involved in oxidative phosphorylation, while genes annotated to canonical glycolysis were repressed in obese BM-MSCs compared with lean ones (Figure 1C). About half of the genes known to be involved in the classical glycolytic pathway showed significant downregulation (false discovery rate [FDR] < 0.1) in obese BM-MSCs (Figure 1D). These data demonstrate that obesity is associated with changes in the molecular signature of BM-MSCs, exhibiting reduced glycolytic capacity and enhanced oxidative phosphorylation. As a corollary, we found several enzymes with oxidoreductase activity upregulated in obese BM-MSCs (e.g., *LDHB*, *AKR1C2*, *P4HA3*) (Figure S1C).

BM-MSC cultures are heterogeneous with respect to differentiation state and include stem cells and committed adipocytic (AD) and osteoblastic (OB) progenitors (James et al., 2015; Post et al., 2008). The metabolic profiles and GO analysis suggest a shift in the population toward decreased stemness and higher metabolic activity and an AD phenotype in obese BM-MSC cultures. To further test this hypothesis, first we found elevated expression levels of AD marker genes (e.g., *PPARG*,

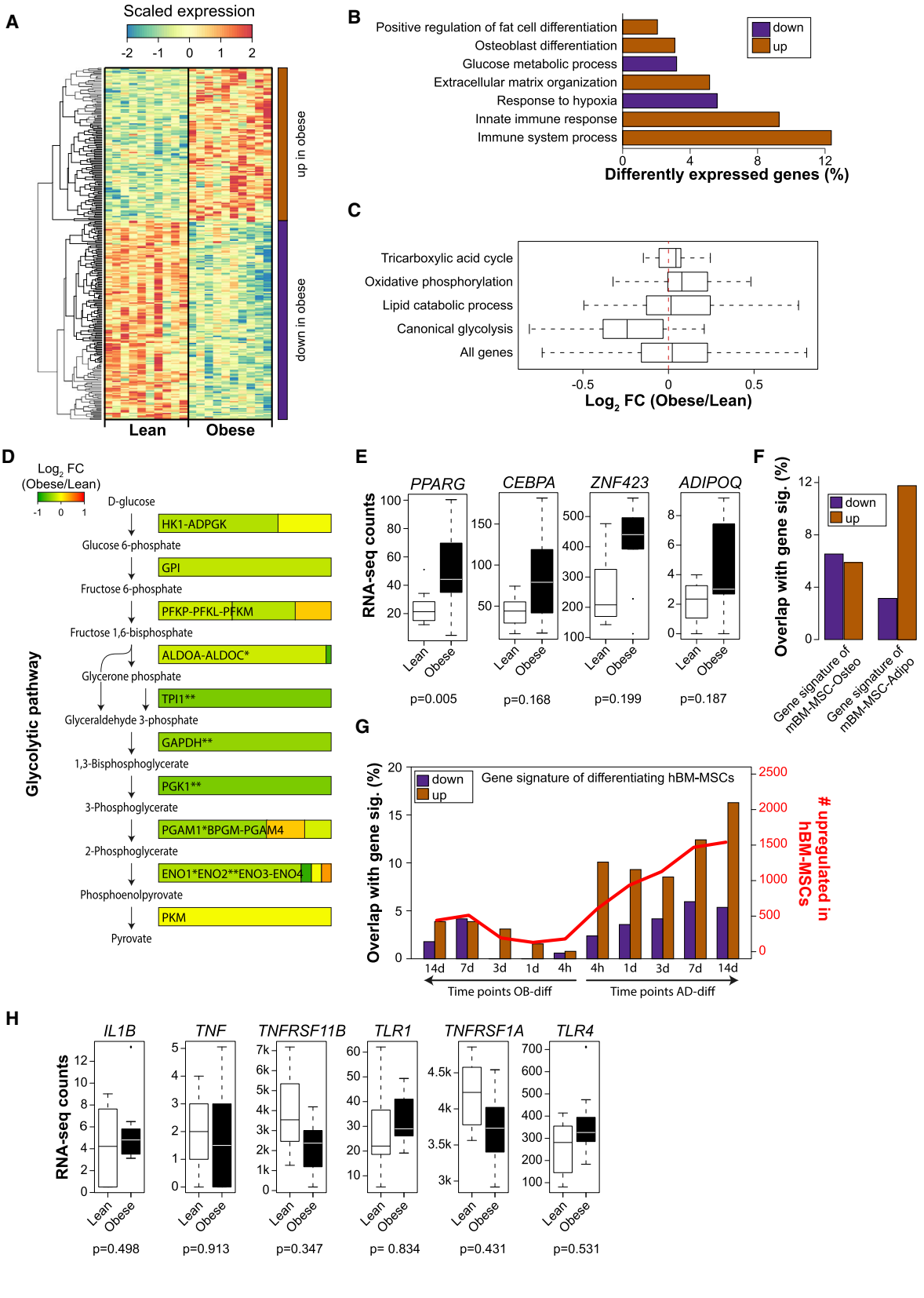

(legend on next page)

CEBPA, *ZNF423*, *ADIPOQ*) in obese compared with lean BM-MSCs (Figure 1E). Second, when focusing on published gene signatures of committed OB (mBM-MSC-Osteo) and AD (mBM-MSC-Adipo) progenitors (Abdallah et al., 2015; Post et al., 2008; Taipaleenmäki et al., 2011), we found that adipocyte- but not osteoblast-associated genes were enriched in obese BM-MSC cultures (Figure 1F). Third, we observed that the upregulated genes in obese BM-MSCs were consistently enriched for genes induced during adipocyte differentiation of human BM-MSCs (hBM-MSCs) (Figure 1G) (Rauch et al., 2019; Twine et al., 2014). Thus, bioinformatic analysis demonstrated evidence of a shift in the molecular phenotype of cultured obese BM-MSCs toward more committed adipocyte progenitors.

Surprisingly, we did not observe increased expression levels of classical pro-inflammatory genes related to Toll-like receptor and NFκB signaling (e.g., *IL1B*, *TNF*, *TNFRSF11B*, *TNFRSF1A*, *TLR4*) in obese compared with lean BM-MSCs, which is opposite to what has been reported in peripheral AT in obesity (Klimcáková et al., 2011) (Figure 1H). These data suggest that BM in obese patients is protected from systemic inflammation and may explain why obesity is associated with low bone turnover and decreased bone resorption activity.

Obesity Leads to Changes in Cellular Composition of BM-MSCs

Because RNA-seq data suggested a decreased stemness with obesity, we investigated stem cell properties of BM-MSC cultures obtained from lean, OW, and obese individuals. The number of colony-forming units-fibroblast (CFUs-f), an *in vitro* surrogate marker for BM-MSCs as well as the short-term proliferation rate of obese BM-MSCs, decreased (Table S4; Figure 2A). The number of cells expressing common stem cell markers of hBM-MSCs, including CD44, CD90, and CD105, did not show any significant changes with obesity (Table S4). However, the number of cells expressing LEPR+, IR+, and C-X-C chemokine receptor (CXCR4+) increased (Figure 2B). These markers were previously reported to be associated with changes in stem cell lineage determination and regulation of immuno-modulatory properties of BM-MSCs (Andres et al., 2013; Miller et al., 2008; Xia et al., 2015; Zhang et al., 2016; Zhou et al., 2014). Furthermore, obese BM-MSCs exhibited enhanced AD differentiation capacity highlighted by the induction levels of AD genes (*PPARG*, *FASN*, *IRS1*) and adipokine (*ADIPOQ*) (Figure 2C) as well as oil red O staining for mature adipocytes (Figure 2D). In addition, obese BM-MSCs showed increased OB differentiation, measured by increased alkaline phosphatase (ALP) activity, alizarin red staining for mineralized matrix formation, and *ALPL* mRNA levels (Figure 2E). Taken together, the *in vitro* data corroborate the observed molecular phenotype identified by RNA-seq and revealed enrichment of committed progenitors in obese BM-MSC cultures. It is plausible that the combined small number of CFU-f and increased number of committed progenitors contribute to low bone turnover state observed in obese subjects, as it leads to progressive failure in the recruitment of new cells needed for bone remodeling. A similar observation was made in a murine model of HFD-induced obesity, in which we and other research groups reported the presence of a decreased CFU-f number and an increased number of AD progenitors (Ambrosi et al., 2017; Tencerova et al., 2018).

Obese BM-MSCs Maintain Insulin Responsiveness

Insulin resistance and high insulin levels are associated with obesity, resulting in its known metabolic complications of diabetes and cardiovascular disease (Czech et al., 2013). Previous studies have demonstrated the presence of an insulin-resistance phenotype at the level of extramedullary adipocytes (Rossmeislová et al., 2013), muscle (Petersen et al., 2007), and liver (Perry et al., 2014) in obese subjects. However, the role of insulin resistance in bone metabolism is not well studied. Thus, we examined insulin signaling and responsiveness in BM-MSCs obtained from lean and obese subjects and compared insulin responsiveness in paired AT-MSCs established from extramedullary subcutaneous AT (SAT) (in a subgroup of ten samples per group from the original cohort of 57 subjects). Interestingly, obese compared with lean BM-MSCs exhibited enhanced insulin-stimulated activation of pAKT(S473) to total AKT, a marker of cellular insulin responsiveness in undifferentiated

Figure 1. Obesity Is Associated with Enrichment of the Molecular Signature of BM-MSCs into Adipocytic Progenitor Cells

Bone marrow stromal stem cell (BM-MSC) cultures were established from lean (n = 10) and obese (n = 10) healthy subjects. RNA was isolated and RNA-seq was performed on undifferentiated cells.

(A) Heatmap showing scaled expression levels from genes differentially expressed between BM-MSCs of lean and obese subjects (n = 10 per group).

(B) Bar plot of Gene Ontology (GO) annotations of obesity-affected genes in BM-MSCs.

(C) Boxplot showing the $\log_2$ fold change of genes belonging to the indicated metabolic process between obese and lean BM-MSC cultures.

(D) Schematic representation of genes enriched in glycolytic pathway expressed in lean versus obese BM-MSC cultures.

(E) Boxplot showing the expression levels of adipocytic marker genes in lean and obese BM-MSCs. *PPARG*, peroxisome proliferator-activated receptor gamma; *CEBPA*, CCAAT/enhancer-binding protein alpha; *ZNF423*, zinc finger protein 423; *ADIPOQ*, adiponectin.

(F) Bar plot representing the overlap of genes that are upregulated (orange) or downregulated (purple) in obese BM-MSCs with gene signatures from adipocyte or osteoblast progenitor cell populations as determined previously (mBM-MSC^{adipo} and mBM-MSC^{osteo}, respectively) (Abdallah et al., 2015; Post et al., 2008).

(G) Bar plot representing the overlap of genes that are upregulated (orange) or downregulated (purple) in obese BM-MSCs with genes being upregulated through the *in vitro* differentiation of human BM-MSCs (hBM-MSCs) to osteoblasts or adipocytes. The red line shows the number of genes upregulated at the indicated time points of *in vitro* differentiation.

(H) Boxplot showing the expression levels of classical pro-inflammatory genes in lean and obese BM-MSCs. *IL1B*, interleukin-1 beta; *TNF*, tumor necrosis factor; *TNFRSF11B*, tumor necrosis factor receptor superfamily member 11B; *TLR1*, Toll-like receptor 1; *TNFRSF1A*, tumor necrosis factor receptor superfamily member 1A; *TLR4*, Toll-like receptor 4.

Data are presented as mean ± SEM; two-tailed unpaired Student's t test.

See also Figure S1.

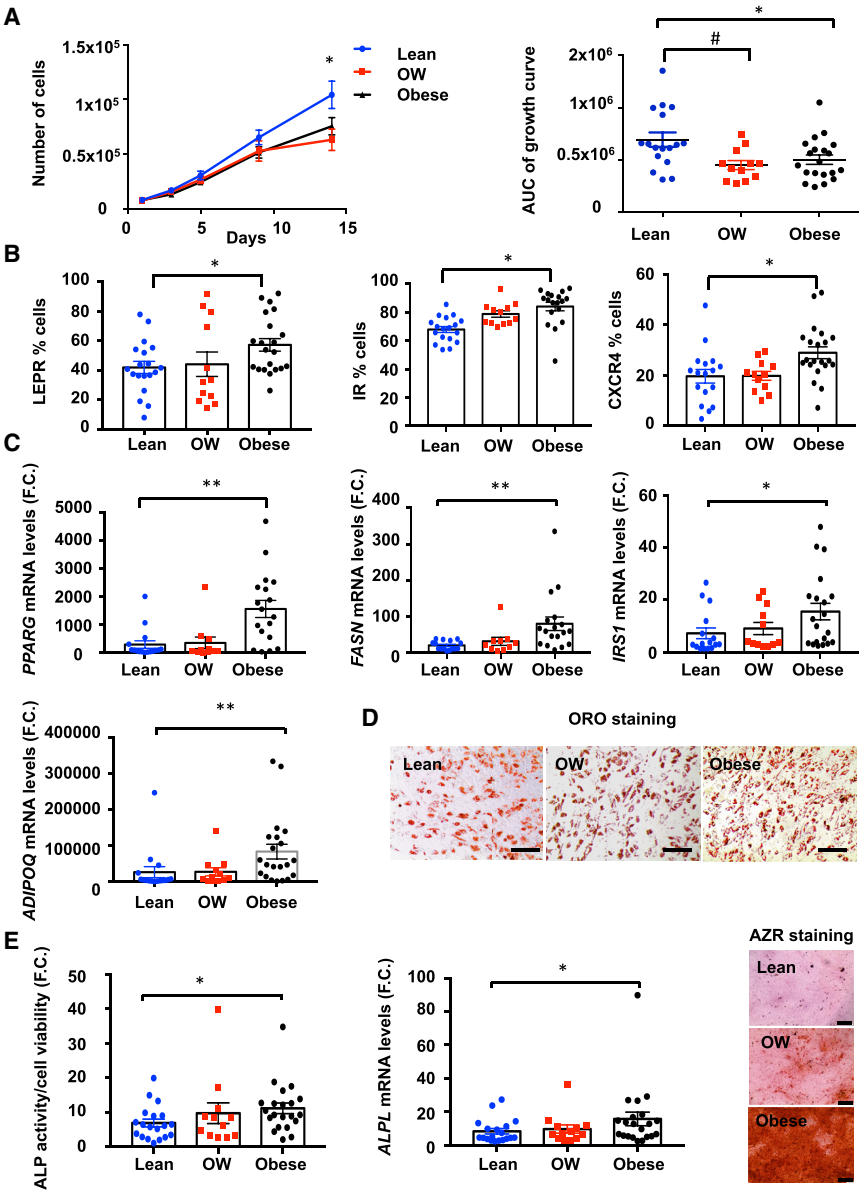

Figure 2. Obesity Leads to Changes in the Cellular Composition of BM-MSCs

BM-MSCs were established from lean (n = 19), overweight (OW) (n = 15), and obese (n = 20) subjects. The cells were examined in undifferentiated state and following adipocyte differentiation (AD) during 10 days.

(A) Short-term proliferative rate and area under the curve (AUC) of BM-MSCs in lean, OW, and obese subjects (n = 15–20). *p < 0.05, lean versus obese; #p < 0.05, lean versus OW.

(B) Screening of stem cell surface marker expression, such as LEPR, IR, and CXCR4, measured using flow cytometry in BM-MSCs isolated from lean, OW, and obese subjects (n = 15–20). *p < 0.05, lean versus obese.

(C) Adipocyte differentiation of BM-MSCs evaluated using gene expression of *PPARG*, *FASN*, *IRS1*, and *ADIPOQ*.

(D) Oil red O staining of mature adipocytes (scale bar, 100 μm; n = 15–20). Data are presented as mean of fold change (F.C.) of gene expression over undifferentiated cells ± SEM; *p < 0.05; **p < 0.01, lean versus obese AD BM-MSCs (two-tailed unpaired Student's t test).

(E) Osteoblast differentiation potential of the BM-MSCs evaluated using quantification of alkaline phosphatase (ALP) activity represented as fold change (F.C.) over non-induced cells (day 7), alizarin staining (scale bar, 400 μm), and gene expression of *ALPL* mRNA levels (n = 15–20); **p < 0.01; ***p < 0.001, lean versus obese CT BM-MSCs; #p < 0.05, lean versus obese OB BM-MSCs (two-tailed unpaired Student's t test).

positively correlated with clinical parameters such as BMI and fasting glucose, supporting the evidence of enhanced insulin signaling in BM-MSCs in obese subjects (Figure S2D).

Our findings suggest that obesity induces insulin resistance in peripheral AT but maintains insulin sensitivity in BM-MSCs. Previous animal studies have investigated the role of insulin signaling in bone homeostasis (Ferron et al., 2010; Fulzele et al., 2010; Wei et al., 2014) using INSR-deficient mice as a model for insulin resistance relevant for insulin deficiency phenotype taking place as a complication of long-standing T2D, which is different from our clinical study with obese subjects who exhibited insulin resistance phenotype but no overt diabetes.

Moreover, the study in obese mice receiving a HFD showed local insulin resistance in bone (Wei et al., 2014). However, insulin signaling was examined in the whole-bone lysate that contains heterogeneous cell populations. These observations do not contradict our findings, as the authors did not examine intrinsic changes in BM-MSCs, and the observed insulin resistance may have been related to microenvironmental factors. Also, the mice examined were overtly diabetic, whereas the human subjects in our study were not. Furthermore, the study

state, and this responsiveness was maintained following AD differentiation (Figures 3A and 3B). On the other hand, obese AT-MSCs from SAT exhibited impaired insulin signaling compared with lean AT-MSCs (Figures 3C and 3D). Moreover, obese AT-MSCs in contrast to BM-MSCs showed a higher expression level of pro-inflammatory genes, lower expression of AD marker genes (Figures 3E, 3F, and 1H, respectively), and decreased number of LEPR+ and IR+ cells in obesity (Figure S2A), supporting previous findings of a negative effect of obesity on the reservoir of functionally active extramedullary AD progenitors (Oñate et al., 2012). Comparison of LEPR and IR expression levels between BM-MSCs and AT-MSCs revealed higher abundance of both markers in BM-MSCs (Figures S2B and S2C), corroborating the existence of significant differences between BMAT and peripheral AT. In addition, IR expression in BM-MSCs was

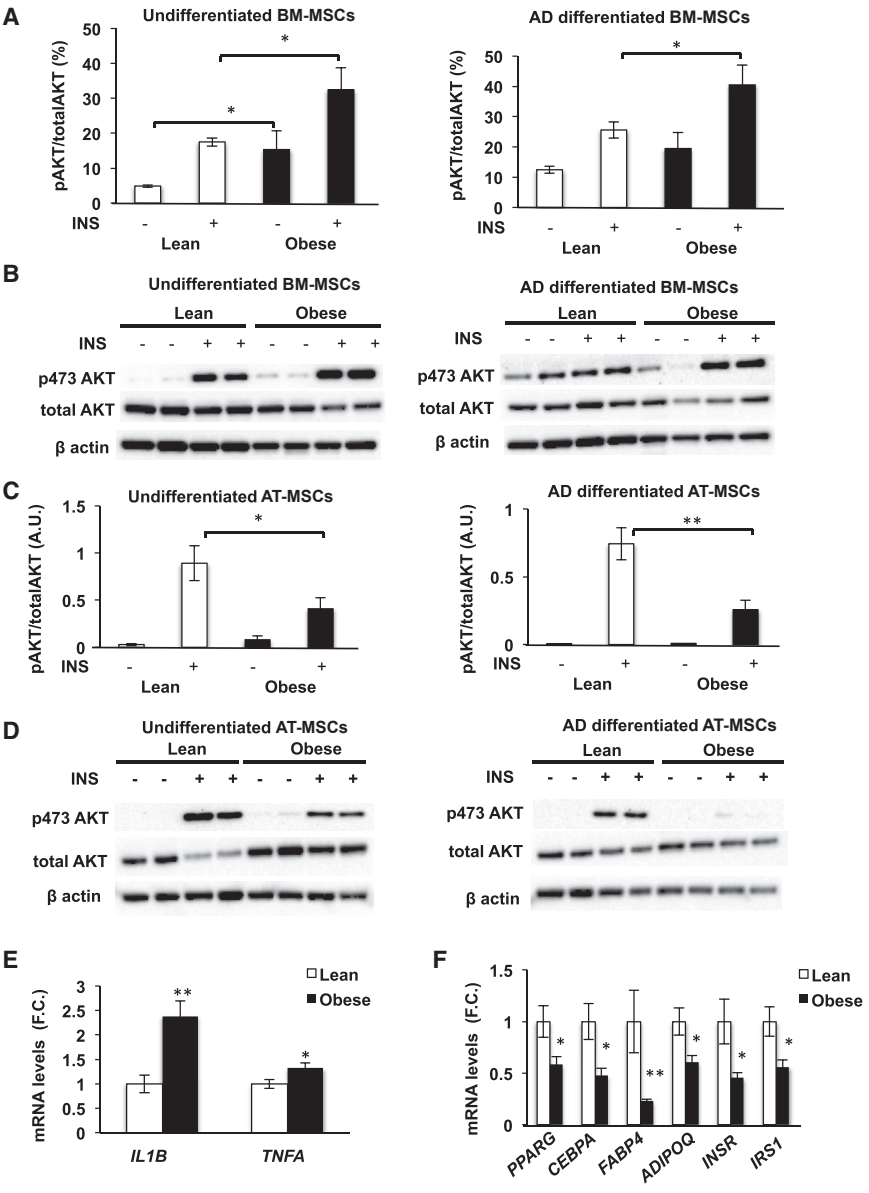

Figure 3. Insulin Signaling Is Enhanced in Obese BM-MSCs

The subgroup of samples of BM-MSCs and adipose-derived stem cells (AT-MSCs) (lean, n = 10; obese, n = 10) was established from the original cohort of 57 subjects. The cells were examined in undifferentiated state and following adipocyte differentiation (AD) during 10 days.

(A) Measurement of pAKT to total AKT in cell lysates of lean and obese BM-MSCs in undifferentiated and following AD differentiation using Immunoplex method (Gowan et al., 2007) (n = 10).

(B) Representative western blots showing insulin-stimulated (100 nM, 15 min) phosphorylation of AKT (p-S473AKT) and total AKT in undifferentiated and AD differentiated BM-MSCs (n = 8 per group).

(C) Densitometry evaluation of western blots measuring insulin stimulation (100 nM) of AKT as p-S473-AKT to total AKT in AT-MSCs in undifferentiated and AD differentiated condition in lean and obese subjects (n = 8 per group).

(D) Representative western blots of p-S473-AKT to total AKT in lean and obese AT-MSCs.

(E and F) Gene expression profile represented as fold change (F.C.) of gene expression of (E) inflammatory genes (*IL1B* and *TNFA*) and (F) adipocytic marker genes (*PPARG*, *CEBPA*, *FABP4*, *ADIPOQ*, *INSR*, *IRS1*) in lean and obese AT-MSC (n = 10).

Data are presented as mean ± SEM; *p < 0.05 and **p < 0.01, lean versus obese (two-tailed unpaired Student's t test).

See also Figure S2.

of Wei et al. (2014) corroborates our hypothesis, as it showed that mice with enhanced insulin signaling in bone are protected from severe systemic insulin resistance phenotype. It is thus plausible that BM maintenance of insulin responsiveness in obese patients allows storage of fat in BM and thus serves as protective mechanism against severe insulin resistance.

IR and LEPR Are Biomarkers for Hypermetabolic State of BM-MSCs

As shown above, obese BM-MSC cultures were enriched for LEPR+ and IR+ cells compared with lean BM-MSCs. To study the *in vivo* relevance of the *in vitro* data, we determined the expression profile of LEPR+ and IR+ cells using *in situ* hybridization in human iliac crest bone biopsies obtained from healthy donors (Figures 4A and 4B). Both IR+ and LEPR+ cells were more abundant in yellow marrow areas packed with adipocytes compared with areas of red marrow filled with hematopoietic cells (Figures 4A and 4B). To study the functional capacity of the cells, we sorted IR+/− and LEPR+/− populations of hBM-MSCs and examined their differentiation potential (Figures S3A and S3B). IR+ and LEPR+ cells exhibited higher AD differentiation capacity (Figures 4C–4F), while IR− and LEPR− cells were more efficient at OB differentiation (Figures 4G–4J), which was altered in INSR-small interfering RNA (siRNA) and LEPR-siRNA transfected cells showing lower AD and enhanced OB differentiation capacity (Figures S4A–S4D). Moreover, IR+ and LEPR+ cells exhibited higher responsiveness to insulin in culture (Figures S4E–S4H), which was reverted with siRNA-mediated silencing of INSR and LEPR (Figures S5A–S5D). In addition, LEPR-siRNA silencing in BM-MSC led to impairment of leptin signaling (Figures S5E–S5H).

Previous studies have demonstrated importance of mitochondrial respiration and oxidative phosphorylation (OXPHOS) in regulation of adipogenesis (Shyh-Chang et al., 2013) and adipocyte commitment, whereas osteoblast commitment is associated with glycolysis (Guntur et al., 2018). Thus, we investigated the bioenergetic profile of IR+ and LEPR+ sorted cells (Figures 4K and 4L). Using Seahorse technology employing the Mito

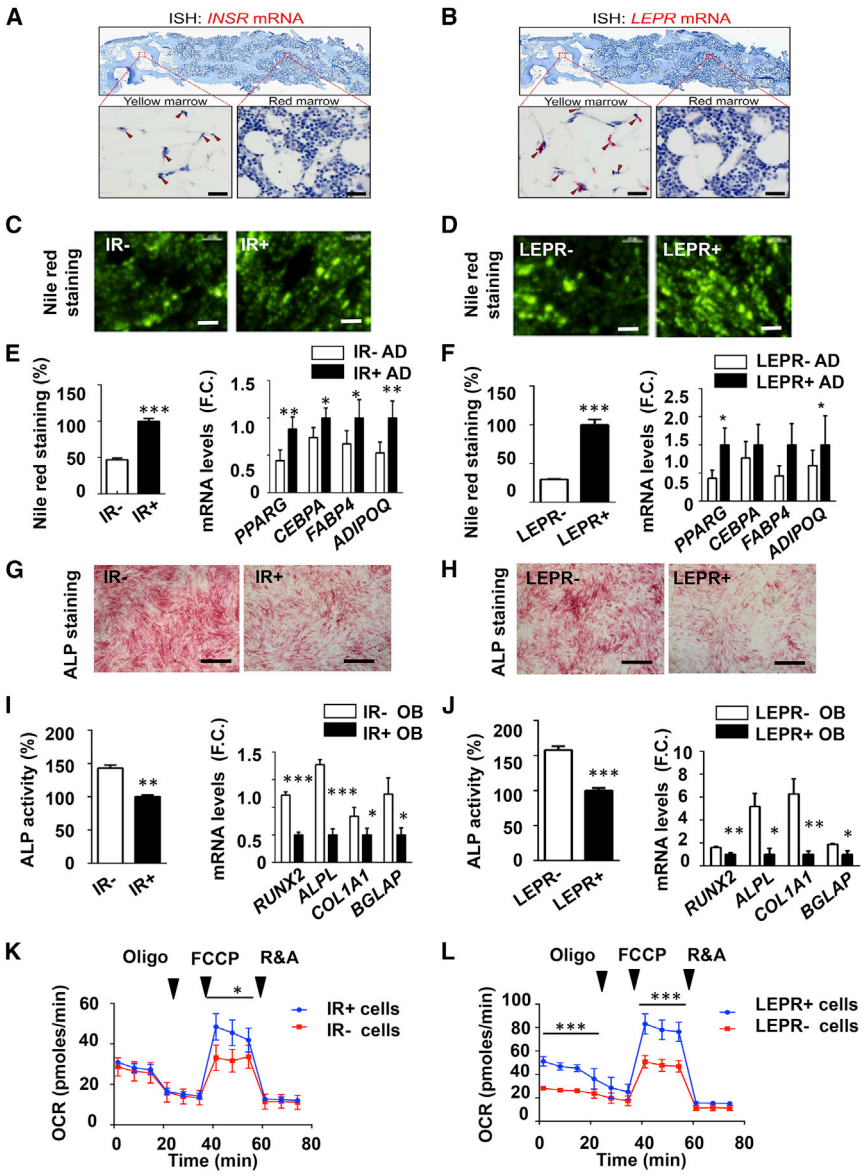

Figure 4. IR+ and LEPR+ as Markers for Metabolically Active Adipocytic Progenitor Cells

Insulin receptor positive (IR+) and leptin receptor positive (LEPR+) cells were sorted using fluorescence-activated cell sorting (FACS) from cultured hBM-MSCs. The cells were examined at baseline and during *in vitro* adipocyte (AD) and osteoblast (OB) differentiation.

(A and B) Representative pictures of *in situ* hybridization (red) of (A) *INSR* and (B) *LEPR* mRNA in human iliac crest bone biopsies of healthy donors. Arrowheads mark IR+ and LEPR+ expressing cells in the yellow marrow (scale bars, 25 μm).

(C and D) Representative pictures of Nile red staining for mature adipocytes in IR+ and IR− cells (C) (scale bar, 100 μm) and in LEPR+ and LEPR− cells (D) sorted from hBM-MSCs (scale bar, 100 μm).

(E) Adipocyte differentiation of IR+ and IR− sorted cells: quantification of Nile red staining for mature adipocytes (left panel) and gene expression of adipocytic marker genes (*PPARG*, *CEBPA*, *FABP4*, *ADIPOQ*) following AD differentiation (right panel).

(F) Adipocyte differentiation of LEPR+ and LEPR− sorted cells: quantification of Nile red staining for mature adipocytes (left panel) and gene expression of adipocytic marker genes (*PPARG*, *CEBPA*, *FABP4*, *ADIPOQ*) following AD differentiation (right panel).

(G and H) Representative pictures of alkaline phosphatase (ALP) staining for mature osteoblasts in (G) IR+ and IR− cells (scale bar, 400 μm) and (H) in LEPR+ and LEPR− cells sorted (scale bar, 400 μm).

(I) Osteoblast differentiation of IR+ and IR− cells: quantification of ALP activity represented as fold change over non-induced cells (left panel) and gene expression of osteoblastic genes (*RUNX2*, *ALPL*, *COL1A1*, *BGLAP*) following OB differentiation (right panel).

(J) Osteoblast differentiation of LEPR+ and LEPR− cells: quantification of ALP activity represented as fold change over non-induced cells (left panel) and gene expression of osteoblastic genes (*RUNX2*, *ALPL*, *COL1A1*, *BGLAP*) following OB differentiation (right panel).

(K and L) Bioenergetic profiling of (K) IR+ and IR− cells and (L) LEPR+ LEPR− cells in Mito stress test measuring mitochondrial oxygen consumption rate (OCR). Oligo, oligomycin; FCCP, carbonyl cyanide-p-trifluoromethoxyphenylhydrazone; R&A, rotenone and antimycin A.

Data are presented as mean ± SEM from three independent experiments. *p < 0.05, **p < 0.01, and ***p < 0.001, positive versus negative cells (two-tailed unpaired Student's t test).

See also Figures S4 and S5.

stress test, we measured cellular OXPHOS reflecting mitochondrial function by determining the oxygen consumption rate (OCR). Undifferentiated IR+ and LEPR+ cells exhibited higher OCRs, which correlates with their AD commitment phenotype (Figures 4K and 4L).

IR+ and LEPR+ Cells Exhibit Accelerated Senescence Phenotype

High levels of OCR and increased oxidative respiratory capacity lead to increased production of reactive oxygen species (ROS), which may promote accelerated cellular senescence (Manolagas, 2010). To examine this hypothesis in IR+ and LEPR+ hBM-MSCs, markers of cellular senescence were determined. Compared with IR− and LEPR− cells, IR+ and LEPR+ cells showed increased expression of senescence-associated genes (*TP53*, *CDKN2A*, *CDKN1A*) and oxidative stress markers (*HMOX1*, *SOD2*, *ALDH1A1*) (Figures 5A and 5B) as well as higher expression of senescence-associated secretory phenotype (SASP) markers that play a role in creating senescence microenvironment (Farr et al., 2016, 2017) (Figures S6A and S6B). In addition, we determined the levels of cellular senescence-associated marker β-galactosidase (β-gal) (Itahana et al., 2013), which

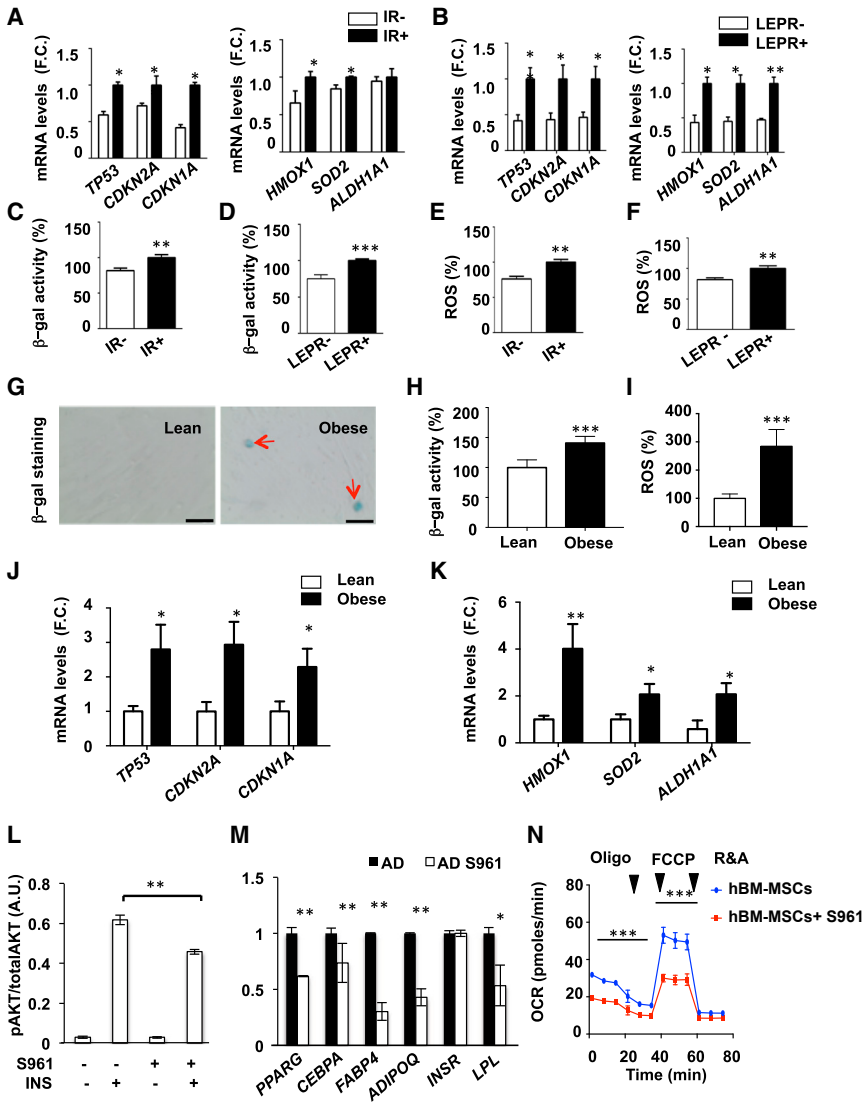

Figure 5. Cultured IR+ and LEPR+ Cells Exhibit Accelerated Senescence Phenotype

IR+ and LEPR+ cells were FACS-sorted from cultured hBM-MSCs.

(A and B) Gene expression of senescence-associated markers (*TP53*, *CDKN2A*, *CDKN1A*) and oxidative stress markers (*HMOX1*, *SOD2*, *ALDH1A1*) in (A) IR+ and IR− cells and (B) in LEPR+ and LEPR− cells.

(C and D) Senescence-associated β-galactosidase (β-gal activity) in (C) IR+ and IR− cells and (D) in LEPR+ and LEPR− cells (n = 3).

(E and F) ROS production following 1 h treatment with H_2O_2 (100 μM) in (E) IR+ and IR− cells and (F) in LEPR+ and LEPR− cells (n = 3). Data are presented as mean ± SEM from three independent experiments. *p < 0.05, **p < 0.01, and ***p < 0.001, positive versus negative cells (two-tailed unpaired Student's t test).

(G) Representative β-gal staining in BM-MSC cultures established from lean and obese subjects. Red arrows mark blue senescent cells (scale bar, 40 μm) (n = 3).

(H) β-gal activity in BM-MSCs from lean and obese subjects (n = 3).

(I) ROS production following 1 h treatment with H_2O_2 (100 μM) in cultured BM-MSCs from lean and obese subjects (n = 3).

(J and K) Gene expression of senescence-associated markers (*TP53*, *CDKN2A*, *CDKN1A*) (J) and oxidative stress markers (*HMOX1*, *SOD2*, *ALDH1A1*) (K) in cultured BM-MSCs from lean and obese subjects (n = 3). Data are presented as mean ± SEM; *p < 0.05, **p < 0.01, and ***p < 0.001, lean versus obese (two-tailed unpaired Student's t test).

(L–N) Effect of treatment with IR antagonist (S961) on AD differentiation and metabolic activity in cultured hBM-MSCs.

(L) Densitometry evaluation of western blot measuring insulin stimulation (100 nM) of AKT as p-S473-AKT to total AKT following S961 treatment (100 nM).

(M) Gene expression of adipocytic marker genes (*PPARG*, *CEBPA*, *FABP4*, *ADIPOQ*, *INSR*, *LPL*) following S961 treatment (100 nM) during AD differentiation.

(N) Bioenergetic profiling of BM-MSCs treated with or without S961 (1 μM) in Mito stress test measuring mitochondrial function (OCR). Oligo, oligomycin; FCCP, carbonyl cyanide-p-trifluoromethoxyphenylhydrazone; R&A, rotenone and antimycin A (n = 3). Data are presented as mean ± SEM; *p < 0.05, **p < 0.01, and ***p < 0.001, non-treated versus S961-treated (two-tailed unpaired Student's t test).

See also Figure S6.

confirmed the presence of high levels of β-gal activity, suggesting an increased number of senescent cells in IR+ and LEPR+ cultures (Figures 5C and 5D). These findings were accompanied by increased ROS production in IR+ and LEPR+ cultures (Figures 5E and 5F). Because obese BM-MSC cultures were enriched for IR+ and LEPR+ cells, we examined the presence of an accelerated cellular senescence phenotype. Obese BM-MSC cultures contained higher number of senescent β-gal+ cells, exhibited higher β-gal activity and increased ROS production (Figures 5G–5I) as well as increased gene expression levels of cellular senescence and oxidative stress markers (Figures 5J and 5K).

Because our results suggest that the presence of enhanced insulin signaling in obese BM-MSCs leads to a hyper-activated metabolic phenotype, we tested whether blocking insulin signaling in BM-MSCs reverses this phenotype. Treatment of BM-MSCs with IR blocker (S961) led to decreased AKT phosphorylation and decreased AD differentiation capacity (Figures 5L and 5M; Figure S6C). Moreover, inhibiting insulin signaling by S961 decreased the OCR of BM-MSCs (Figure 5N). These results were further confirmed by siRNA-mediated silencing of INSR in BM-MSC cultures that resulted in lower metabolic activity and OCR, decreased gene expression levels of AD markers, as well as senescence and oxidative stress markers in INSR-siRNA compared with SCR-siRNA transfected cells (Figures S6D and S6E).

A number of studies have reported that enhanced insulin signaling leads to an accelerated senescence phenotype. In

hematopoietic stem cells overexpressing IR, increased proliferation and differentiation capacity of the progenitor cells leading to cellular senescence have been observed (Kharas et al., 2010). Moreover, the basal IR tyrosine kinase activity is upregulated during oxidative stress associated with a cellular senescence phenotype (Schmitt et al., 2005). Furthermore, the role of enhanced insulin signaling in age-related degenerative diseases has been demonstrated in animals deficient in IR that exhibited downregulation of cellular metabolism and oxidative stress signaling and extended healthy lifespan (Dröge, 2005).

Limitations of the Study

Our study had some limitations. The study was performed in men as a continuation of preclinical studies performed in male mice by others and us (Doucette et al., 2015; Scheller et al., 2016; Tencerova et al., 2018). However, a similar study investigating cellular changes in a female cohort is needed. We have examined the hypothesis of presence of intrinsic defects in BM-MSCs using cultured cells. Although *in vitro* culture conditions may influence cellular phenotype, a number of previous studies have demonstrated that *in vitro* cultured preadipocytes, adipocytes, or muscle cells maintained metabolic characteristics of the donor (Jiang et al., 2013; Kase et al., 2015; Tchkonia et al., 2006; van Tienen et al., 2011). This clinical study was performed in BM-MSCs obtained from the iliac crest, which is recognized as a standard sampling site for bone biopsies in healthy subjects and is considered to reflect the status of skeletal bone remodeling. Even though obesity affects the skeleton in a site-specific manner, using the iliac crest as a source of bone biopsy has the advantage of being a standardized site that is used by the majority of investigators, allowing comparison of results.

Overall Perspective

Our study provides an understanding of obesity-associated bone fragility as mediated by enhanced insulin signaling and enrichment for AD progenitor cells in the BM microenvironment. These changes lead to increased glucose use and enhanced mitochondrial OXPHOS, producing ROS and causing BM-MSC stem cell exhaustion and the creation of a senescent BM microenvironment conducive to bone fragility. An increased number of senescent cells has been reported in AT-MSCs of obese subjects (Tchkonia et al., 2010), and we extend these findings to BM-MSCs. Our data identify increased insulin signaling in BM-MSCs as a target for a potential tailored therapy in obesity and T2D-associated bone fragility and support a previous study by Farr et al. (2017) showing that elimination of senescent cells in mice prevented age-related bone loss.

What is the mechanism of maintenance of BM insulin signaling in the context of obesity-associated peripheral insulin resistance? Our study provides a plausible explanation, as it demonstrates the presence of multiple factors: the increased number of IR-positive progenitors, increased expression of IR, the known presence of a BM barrier (Mangialardi et al., 2013; Shadduck et al., 1989), and the protection of the inflammatory response by the hematopoietic cells (Tencerova et al., 2018) possibly by the anti-inflammatory and immunosuppressive characteristics of BM-MSCs being part of the innate immune response (Marigo and Dazzi, 2011). Teleologically, absence of insulin resistance in BM-MSC may represent an adaptive response to meet the energy requirement needed for defense against infection (Wolowczuk et al., 2008). Finally, our findings can explain the presence of low bone turnover in obese and T2D patients leading to accumulation of fatigue damage, decreased bone material quality, and increased risk for bone fragility (Burr et al., 1997).

Recent studies in healthy individuals revealed positive biological effects of metabolic slowing following a caloric restriction program for 2 years (Heilbronn and Ravussin, 2003; Redman et al., 2018) and provide an interesting perspective for the prevention of accelerated aging observed in metabolically active organs, including the skeletal system. Beneficial effects of caloric restriction or selective insulin inhibition on bone stem cell functionality and bone fragility in obese and T2D patients remain to be determined.

STAR★METHODS

Detailed methods are provided in the online version of this paper and include the following:

- KEY RESOURCES TABLE
- CONTACT FOR REAGENT AND RESOURCE SHARING
- EXPERIMENTAL MODEL AND SUBJECT DETAILS
  - Human subjects
  - Isolation and culture of bone marrow stromal stem cells from bone marrow aspirates
  - Isolation and culture of adipose-derived stromal cells (AT-MSCs) from needle biopsy
- METHOD DETAILS
  - Clinical investigations
  - Oral glucose tolerance test (OGTT)
  - DXA scans
  - Biochemical analyses
  - Flow cytometry
  - Cells proliferation
  - Colony forming unit-fibroblast (CFU-f) assay
  - *In vitro* differentiation
  - Insulin responsiveness of BM-MSCs and AT-MSCs
  - Senescence-associated β-galactosidase (β-gal) activity assay
  - Senescence-associated β-galactosidase Staining
  - Cellular Reactive Oxygen Species (ROS) Detection assay
  - Mitochondrial stress test
  - Treatment of BM-MSCs with S961 (insulin receptor antagonist)
  - siRNA transfection of hBM-MSCs
  - Treatment of transfected and sorted hBM-MSCs with insulin and leptin
  - RNA extraction and Real time qRT-PCR
  - RNA sequencing of BM-MSCs
  - Western blot
  - Multiplexed ELISA of Protein Phosphorylation
- QUANTIFICATION AND STATISTICAL ANALYSIS
  - Statistical analyses
- DATA AND SOFTWARE AVAILABILITY

SUPPLEMENTAL INFORMATION

Supplemental Information can be found online at https://doi.org/10.1016/j.celrep.2019.04.066.

ACKNOWLEDGMENTS

We are grateful to Lone Hansen, Charlotte Bøtchiær Olsen, and Anette Riis Madsen from the Endocrine Research Unit, Department of Endocrinology, and Lone Christiansen from the Department of Pathology at Odense University Hospital for their excellent technical assistance. We thank Dr. Susanne Mandrup for providing infrastructure for RNA-seq. Sequencing was carried out at the Villum Center for Bioanalytical Sciences, Functional Genomics & Metabolism Research Unit, University of Southern Denmark. We thank Tenna P. Mortensen and Ronni Nielsen for sequencing assistance. Furthermore, we thank Dr. Kate Lambersten for assistance with the Immunoplex platform (Mesoscale). We also thank Justyna Kowal for great help with the Operetta imaging system and Dr. Myriam Aouadi for helpful discussions and suggestions. This work was supported by a fellowship grant from the Danish Diabetes Academy supported by the Novo Nordisk Foundation (M.T.) and the Novo Nordisk Foundation (NNF18OC0034186 to M.K.), Lundbeck Foundation (R266-2017-4250 to M.K.), the Danish Independent Research Council (DFF-1333-00283 to M.F.), Region Syddanmarks (J.-J.L.L.), and a research grant from Odense University Hospital (R29-A1374 to M.T.).

AUTHOR CONTRIBUTIONS

M.T. and M.K. conceived the project. M.T., T.K.N., F.F., and D.A. performed the *in vitro* experiments and collected and analyzed data. M.F., M.K., J.-J.L.L., and K.H. recruited and performed the clinical examinations of the participants. A.K.H. and A.R. performed RNA-seq biostatistical analyses. T.L.A. performed *in situ* hybridization analyses of human bone specimens, which C.E. collected from healthy donors. J.S.M. performed the biochemical analyses of bone turnover markers. M.T. and M.K. designed and supervised the study and wrote the manuscript. All authors revised and approved the manuscript.

DECLARATION OF INTERESTS

The authors declare no competing interests.

Received: December 6, 2018
Revised: March 6, 2019
Accepted: April 12, 2019
Published: May 14, 2019

REFERENCES

Abdallah, B.M., and Kassem, M. (2012). New factors controlling the balance between osteoblastogenesis and adipogenesis. Bone *50*, 540–545.

Abdallah, B.M., Haack-Sørensen, M., Burns, J.S., Elsnab, B., Jakob, F., Hokland, P., and Kassem, M. (2005). Maintenance of differentiation potential of human bone marrow mesenchymal stem cells immortalized by human telomerase reverse transcriptase gene despite [corrected] extensive proliferation. Biochem. Biophys. Res. Commun. *326*, 527–538.

Abdallah, B.M., Haack-Sørensen, M., Fink, T., and Kassem, M. (2006). Inhibition of osteoblast differentiation but not adipocyte differentiation of mesenchymal stem cells by sera obtained from aged females. Bone *39*, 181–188.

Abdallah, B.M., Al-Shammary, A., Skagen, P., Abu Dawud, R., Adjaye, J., Aldahmash, A., and Kassem, M. (2015). CD34 defines an osteoprogenitor cell population in mouse bone marrow stromal cells. Stem Cell Res. (Amst.) *15*, 449–458.

Adler, B.J., Kaushansky, K., and Rubin, C.T. (2014). Obesity-driven disruption of haematopoiesis and the bone marrow niche. Nat. Rev. Endocrinol. *10*, 737–748.

Ambrosi, T.H., Scialdone, A., Graja, A., Gohlke, S., Jank, A.M., Bocian, C., Woelk, L., Fan, H., Logan, D.W., Schurmann, A., et al. (2017). Adipocyte accumulation in the bone marrow during obesity and aging impairs stem cell-based hematopoietic and bone regeneration. Cell Stem Cell *20*, 771–784.e6.

Andres, S.F., Simmons, J.G., Mah, A.T., Santoro, M.A., Van Landeghem, L., and Lund, P.K. (2013). Insulin receptor isoform switching in intestinal stem cells, progenitors, differentiated lineages and tumors: evidence that IR-B limits proliferation. J. Cell Sci. *126*, 5645–5656.

Anisimov, V.N. (2003). Insulin/IGF-1 signaling pathway driving aging and cancer as a target for pharmacological intervention. Exp. Gerontol. *38*, 1041–1049.

Blüher, M., Michael, M.D., Peroni, O.D., Ueki, K., Carter, N., Kahn, B.B., and Kahn, C.R. (2002). Adipose tissue selective insulin receptor knockout protects against obesity and obesity-related glucose intolerance. Dev. Cell *3*, 25–38.

Blüher, M., Kahn, B.B., and Kahn, C.R. (2003). Extended longevity in mice lacking the insulin receptor in adipose tissue. Science *299*, 572–574.

Boskey, A.L., and Imbert, L. (2017). Bone quality changes associated with aging and disease: a review. Ann. N Y Acad. Sci. *1410*, 93–106.

Bredella, M.A., Torriani, M., Ghomi, R.H., Thomas, B.J., Brick, D.J., Gerweck, A.V., Rosen, C.J., Klibanski, A., and Miller, K.K. (2011). Vertebral bone marrow fat is positively associated with visceral fat and inversely associated with IGF-1 in obese women. Obesity (Silver Spring) *19*, 49–53.

Burr, D.B., Forwood, M.R., Fyhrie, D.P., Martin, R.B., Schaffler, M.B., and Turner, C.H. (1997). Bone microdamage and skeletal fragility in osteoporotic and stress fractures. J. Bone Miner. Res. *12*, 6–15.

Chan, C.K., Seo, E.Y., Chen, J.Y., Lo, D., McArdle, A., Sinha, R., Tevlin, R., Seita, J., Vincent-Tompkins, J., Wearda, T., et al. (2015). Identification and specification of the mouse skeletal stem cell. Cell *160*, 285–298.

Chen, L., Hu, H., Qiu, W., Shi, K., and Kassem, M. (2018). Actin depolymerization enhances adipogenic differentiation in human stromal stem cells. Stem Cell Res. (Amst.) *29*, 76–83.

Cinti, S., Eberbach, S., Castellucci, M., and Accili, D. (1998). Lack of insulin receptors affects the formation of white adipose tissue in mice. A morphometric and ultrastructural analysis. Diabetologia *41*, 171–177.

Czech, M.P., Tencerova, M., Pedersen, D.J., and Aouadi, M. (2013). Insulin signalling mechanisms for triacylglycerol storage. Diabetologia *56*, 949–964.

Doucette, C.R., Horowitz, M.C., Berry, R., MacDougald, O.A., Anunciado-Koza, R., Koza, R.A., and Rosen, C.J. (2015). A high fat diet increases bone marrow adipose tissue (MAT) but does not alter trabecular or cortical bone mass in C57BL/6J mice. J. Cell. Physiol. *230*, 2032–2037.

Dröge, W. (2005). Oxidative aging and insulin receptor signaling. J. Gerontol. A Biol. Sci. Med. Sci. *60*, 1378–1385.

Farr, J.N., Fraser, D.G., Wang, H., Jaehn, K., Ogrodnik, M.B., Weivoda, M.M., Drake, M.T., Tchkonia, T., LeBrasseur, N.K., Kirkland, J.L., et al. (2016). Identification of senescent cells in the bone microenvironment. J. Bone Miner. Res. *31*, 1920–1929.

Farr, J.N., Xu, M., Weivoda, M.M., Monroe, D.G., Fraser, D.G., Onken, J.L., Negley, B.A., Sfeir, J.G., Ogrodnik, M.B., Hachfeld, C.M., et al. (2017). Targeting cellular senescence prevents age-related bone loss in mice. Nat. Med. *23*, 1072–1079.

Ferron, M., Wei, J., Yoshizawa, T., Del Fattore, A., DePinho, R.A., Teti, A., Ducy, P., and Karsenty, G. (2010). Insulin signaling in osteoblasts integrates bone remodeling and energy metabolism. Cell *142*, 296–308.

Fulzele, K., Riddle, R.C., DiGirolamo, D.J., Cao, X., Wan, C., Chen, D., Faugere, M.C., Aja, S., Hussain, M.A., Brüning, J.C., and Clemens, T.L. (2010). Insulin receptor signaling in osteoblasts regulates postnatal bone acquisition and body composition. Cell *142*, 309–319.

Gimble, J.M., Zvonic, S., Floyd, Z.E., Kassem, M., and Nuttall, M.E. (2006). Playing with bone and fat. J. Cell. Biochem. *98*, 251–266.

Gonnelli, S., Caffarelli, C., and Nuti, R. (2014). Obesity and fracture risk. Clin. Cases Miner. Bone Metab. *11*, 9–14.

Gowan, S.M., Hardcastle, A., Hallsworth, A.E., Valenti, M.R., Hunter, L.J., de Haven Brandon, A.K., Garrett, M.D., Raynaud, F., Workman, P., Aherne, W., and Eccles, S.A. (2007). Application of meso scale technology for the

measurement of phosphoproteins in human tumor xenografts. Assay Drug Dev. Technol. *5*, 391–401.

Guntur, A.R., Gerencser, A.A., Le, P.T., DeMambro, V.E., Bornstein, S.A., Mookerjee, S.A., Maridas, D.E., Clemmons, D.E., Brand, M.D., and Rosen, C.J. (2018). Osteoblast-like MC3T3-E1 cells prefer glycolysis for ATP production but adipocyte-like 3T3-L1 cells prefer oxidative phosphorylation. J. Bone Miner. Res. *33*, 1052–1065.

Hayden, J.M., Mohan, S., and Baylink, D.J. (1995). The insulin-like growth factor system and the coupling of formation to resorption. Bone *17* (*2, Suppl*), 93S–98S.

Heilbronn, L.K., and Ravussin, E. (2003). Calorie restriction and aging: review of the literature and implications for studies in humans. Am. J. Clin. Nutr. *78*, 361–369.

Itahana, K., Itahana, Y., and Dimri, G.P. (2013). Colorimetric detection of senescence-associated β galactosidase. Methods Mol. Biol. *965*, 143–156.

Jafari, A., Qanie, D., Andersen, T.L., Zhang, Y., Chen, L., Postert, B., Parsons, S., Ditzel, N., Khosla, S., Johansen, H.T., et al. (2017). Legumain regulates differentiation fate of human bone marrow stromal cells and is altered in postmenopausal osteoporosis. Stem Cell Reports *8*, 373–386.

James, S., Fox, J., Afsari, F., Lee, J., Clough, S., Knight, C., Ashmore, J., Ashton, P., Preham, O., Hoogduijn, M., et al. (2015). Multiparameter analysis of human bone marrow stromal cells identifies distinct immunomodulatory and differentiation-competent subtypes. Stem Cell Reports *4*, 1004–1015.

Jiang, L.Q., Duque-Guimaraes, D.E., Machado, U.F., Zierath, J.R., and Krook, A. (2013). Altered response of skeletal muscle to IL-6 in type 2 diabetic patients. Diabetes *62*, 355–361.

Kase, E.T., Feng, Y.Z., Badin, P.M., Bakke, S.S., Laurens, C., Coue, M., Langin, D., Gaster, M., Thoresen, G.H., Rustan, A.C., and Moro, C. (2015). Primary defects in lipolysis and insulin action in skeletal muscle cells from type 2 diabetic individuals. Biochim. Biophys. Acta *1851*, 1194–1201.

Kassem, M., and Marie, P.J. (2011). Senescence-associated intrinsic mechanisms of osteoblast dysfunctions. Aging Cell *10*, 191–197.

Kharas, M.G., Okabe, R., Ganis, J.J., Gozo, M., Khandan, T., Paktinat, M., Gilliland, D.G., and Gritsman, K. (2010). Constitutively active AKT depletes hematopoietic stem cells and induces leukemia in mice. Blood *115*, 1406–1415.

Klimcáková, E., Roussel, B., Márquez-Quiñones, A., Kovácová, Z., Kovácíková, M., Combes, M., Siklová-Vítková, M., Hejnová, J., Srámková, P., Bouloumié, A., et al. (2011). Worsening of obesity and metabolic status yields similar molecular adaptations in human subcutaneous and visceral adipose tissue: decreased metabolism and increased immune response. J. Clin. Endocrinol. Metab. *96*, E73–E82.

LaFever, L., and Drummond-Barbosa, D. (2005). Direct control of germline stem cell division and cyst growth by neural insulin in Drosophila. Science *309*, 1071–1073.

Laschober, G.T., Brunauer, R., Jamnig, A., Fehrer, C., Greiderer, B., and Lepperdinger, G. (2009). Leptin receptor/CD295 is upregulated on primary human mesenchymal stem cells of advancing biological age and distinctly marks the subpopulation of dying cells. Exp. Gerontol. *44*, 57–62.

Lassen, N.E., Andersen, T.L., Pløen, G.G., Søe, K., Hauge, E.M., Harving, S., Eschen, G.E.T., and Delaisse, J.M. (2017). Coupling of Bone Resorption and Formation in Real Time: New Knowledge Gained From Human Haversian BMUs. J. Bone Miner. Res. *32*, 1395–1405.

Love, M.I., Huber, W., and Anders, S. (2014). Moderated estimation of fold change and dispersion for RNA-seq data with DESeq2. Genome Biol. *15*, 550.

Mangialardi, G., Katare, R., Oikawa, A., Meloni, M., Reni, C., Emanueli, C., and Madeddu, P. (2013). Diabetes causes bone marrow endothelial barrier dysfunction by activation of the RhoA-Rho-associated kinase signaling pathway. Arterioscler. Thromb. Vasc. Biol. *33*, 555–564.

Manolagas, S.C. (2010). From estrogen-centric to aging and oxidative stress: a revised perspective of the pathogenesis of osteoporosis. Endocr. Rev. *31*, 266–300.

Marigo, I., and Dazzi, F. (2011). The immunomodulatory properties of mesenchymal stem cells. Semin. Immunopathol. *33*, 593–602.

Miller, R.J., Banisadr, G., and Bhattacharyya, B.J. (2008). CXCR4 signaling in the regulation of stem cell migration and development. J. Neuroimmunol. *198*, 31–38.

Napoli, N., Chandran, M., Pierroz, D.D., Abrahamsen, B., Schwartz, A.V., and Ferrari, S.L.; IOF Bone and Diabetes Working Group (2017). Mechanisms of diabetes mellitus-induced bone fragility. Nat. Rev. Endocrinol. *13*, 208–219.

Naveiras, O., Nardi, V., Wenzel, P.L., Hauschka, P.V., Fahey, F., and Daley, G.Q. (2009). Bone-marrow adipocytes as negative regulators of the haematopoietic microenvironment. Nature *460*, 259–263.

Oikawa, A., Siragusa, M., Quaini, F., Mangialardi, G., Katare, R.G., Caporali, A., van Buul, J.D., van Alphen, F.P., Graiani, G., Spinetti, G., et al. (2010). Diabetes mellitus induces bone marrow microangiopathy. Arterioscler. Thromb. Vasc. Biol. *30*, 498–508.

Oñate, B., Vilahur, G., Ferrer-Lorente, R., Ybarra, J., Díez-Caballero, A., Ballesta-López, C., Moscatiello, F., Herrero, J., and Badimon, L. (2012). The subcutaneous adipose tissue reservoir of functionally active stem cells is reduced in obese patients. FASEB J. *26*, 4327–4336.

Patro, R., Duggal, G., Love, M.I., Irizarry, R.A., and Kingsford, C. (2017). Salmon provides fast and bias-aware quantification of transcript expression. Nat. Methods *14*, 417–419.

Perry, R.J., Samuel, V.T., Petersen, K.F., and Shulman, G.I. (2014). The role of hepatic lipids in hepatic insulin resistance and type 2 diabetes. Nature *510*, 84–91.

Petersen, K.F., Dufour, S., Savage, D.B., Bilz, S., Solomon, G., Yonemitsu, S., Cline, G.W., Befroy, D., Zemany, L., Kahn, B.B., et al. (2007). The role of skeletal muscle insulin resistance in the pathogenesis of the metabolic syndrome. Proc. Natl. Acad. Sci. U S A *104*, 12587–12594.

Post, S., Abdallah, B.M., Bentzon, J.F., and Kassem, M. (2008). Demonstration of the presence of independent pre-osteoblastic and pre-adipocytic cell populations in bone marrow-derived mesenchymal stem cells. Bone *43*, 32–39.

Qiu, W., Andersen, T.E., Bollerslev, J., Mandrup, S., Abdallah, B.M., and Kassem, M. (2007). Patients with high bone mass phenotype exhibit enhanced osteoblast differentiation and inhibition of adipogenesis of human mesenchymal stem cells. J. Bone Miner. Res. *22*, 1720–1731.

Rauch, A., Haakonsson, A.K., Madsen, J.G.S., Larsen, M., Foss, I., Madsen, M.R., Van Hauwaert, E.L., Wiwie, C., Jespersen, N.Z., Tencerova, M., et al. (2019). Osteogenesis depends on commissioning of a network of stem cell transcription factors that act as repressors of adipogenesis. Nat. Genet. *51*, 716–727.

Redman, L.M., Smith, S.R., Burton, J.H., Martin, C.K., Il'yasova, D., and Ravussin, E. (2018). Metabolic slowing and reduced oxidative damage with sustained caloric restriction support the rate of living and oxidative damage theories of aging. Cell Metab. *27*, 805–815.e4.

Rossmeislová, L., Malisová, L., Kracmerová, J., Tencerová, M., Kovácová, Z., Koc, M., Siklová-Vítková, M., Viquerie, N., Langin, D., and Stich, V. (2013). Weight loss improves the adipogenic capacity of human preadipocytes and modulates their secretory profile. Diabetes *62*, 1990–1995.

Rubin, C.T., Capilla, E., Luu, Y.K., Busa, B., Crawford, H., Nolan, D.J., Mittal, V., Rosen, C.J., Pessin, J.E., and Judex, S. (2007). Adipogenesis is inhibited by brief, daily exposure to high-frequency, extremely low-magnitude mechanical signals. Proc. Natl. Acad. Sci. USA *104*, 17879–17884.

Scheller, E.L., Khoury, B., Moller, K.L., Wee, N.K., Khandaker, S., Kozloff, K.M., Abrishami, S.H., Zamarron, B.F., and Singer, K. (2016). Changes in skeletal integrity and marrow adiposity during high-fat diet and after weight loss. Front. Endocrinol. (Lausanne) *7*, 102.

Schmitt, T.L., Hotz-Wagenblatt, A., Klein, H., and Dröge, W. (2005). Interdependent regulation of insulin receptor kinase activity by ADP and hydrogen peroxide. J. Biol. Chem. *280*, 3795–3801.

Shadduck, R.K., Waheed, A., and Wing, E.J. (1989). Demonstration of a blood-bone marrow barrier to macrophage colony-stimulating factor. Blood *73*, 68–73.

Shyh-Chang, N., Daley, G.Q., and Cantley, L.C. (2013). Stem cell metabolism in tissue development and aging. Development *140*, 2535–2547.

Taipaleenmäki, H., Abdallah, B.M., AlDahmash, A., Säämänen, A.M., and Kassem, M. (2011). Wnt signalling mediates the cross-talk between bone marrow derived pre-adipocytic and pre-osteoblastic cell populations. Exp. Cell Res. *317*, 745–756.

Tchkonia, T., Giorgadze, N., Pirtskhalava, T., Thomou, T., DePonte, M., Koo, A., Forse, R.A., Chinnappan, D., Martin-Ruiz, C., von Zglinicki, T., and Kirkland, J.L. (2006). Fat depot-specific characteristics are retained in strains derived from single human preadipocytes. Diabetes *55*, 2571–2578.

Tchkonia, T., Morbeck, D.E., Von Zglinicki, T., Van Deursen, J., Lustgarten, J., Scrable, H., Khosla, S., Jensen, M.D., and Kirkland, J.L. (2010). Fat tissue, aging, and cellular senescence. Aging Cell *9*, 667–684.

Tencerova, M., and Kassem, M. (2016). The bone marrow-derived stromal cells: commitment and regulation of adipogenesis. Front. Endocrinol. (Lausanne) *7*, 127.

Tencerova, M., Figeac, F., Ditzel, N., Taipaleenmäki, H., Nielsen, T.K., and Kassem, M. (2018). High-fat diet-induced obesity promotes expansion of bone marrow adipose tissue and impairs skeletal stem cell functions in mice. J. Bone Miner. Res. *33*, 1154–1165.

Tonks, K.T., White, C.P., Center, J.R., Samocha-Bonet, D., and Greenfield, J.R. (2017). Bone turnover is suppressed in insulin resistance, independent of adiposity. J. Clin. Endocrinol. Metab. *102*, 1112–1121.

Twine, N.A., Chen, L., Pang, C.N., Wilkins, M.R., and Kassem, M. (2014). Identification of differentiation-stage specific markers that define the ex vivo osteoblastic phenotype. Bone *67*, 23–32.

van Tienen, F.H., van der Kallen, C.J., Lindsey, P.J., Wanders, R.J., van Greevenbroek, M.M., and Smeets, H.J. (2011). Preadipocytes of type 2 diabetes subjects display an intrinsic gene expression profile of decreased differentiation capacity. Int. J. Obes. *35*, 1154–1164.

Wardlaw, G.M. (1996). Putting body weight and osteoporosis into perspective. Am. J. Clin. Nutr. *63* (*3, Suppl*), 433S–436S.

Wei, J., Ferron, M., Clarke, C.J., Hannun, Y.A., Jiang, H., Blaner, W.S., and Karsenty, G. (2014). Bone-specific insulin resistance disrupts whole-body glucose homeostasis via decreased osteocalcin activation. J. Clin. Invest. *124*, 1–13.

Wolowczuk, I., Verwaerde, C., Viltart, O., Delanoye, A., Delacre, M., Pot, B., and Grangette, C. (2008). Feeding our immune system: impact on metabolism. Clin. Dev. Immunol. *2008*, 639803.

Wu, M., Neilson, A., Swift, A.L., Moran, R., Tamagnine, J., Parslow, D., Armistead, S., Lemire, K., Orrell, J., Teich, J., et al. (2007). Multiparameter metabolic analysis reveals a close link between attenuated mitochondrial bioenergetic function and enhanced glycolysis dependency in human tumor cells. Am. J. Physiol. Cell Physiol. *292*, C125–C136.

Xia, P., Wang, S., Du, Y., Huang, G., Satoh, T., Akira, S., and Fan, Z. (2015). Insulin-InsR signaling drives multipotent progenitor differentiation toward lymphoid lineages. J. Exp. Med. *212*, 2305–2321.

Yue, R., Zhou, B.O., Shimada, I.S., Zhao, Z., and Morrison, S.J. (2016). Leptin receptor promotes adipogenesis and reduces osteogenesis by regulating mesenchymal stromal cells in adult bone marrow. Cell Stem Cell *18*, 782–796.

Zhang, Y., Dépond, M., He, L., Foudi, A., Kwarteng, E.O., Lauret, E., Plo, I., Desterke, C., Dessen, P., Fujii, N., et al. (2016). CXCR4/CXCL12 axis counteracts hematopoietic stem cell exhaustion through selective protection against oxidative stress. Sci. Rep. *6*, 37827.

Zhou, B.O., Yue, R., Murphy, M.M., Peyer, J.G., and Morrison, S.J. (2014). Leptin-receptor-expressing mesenchymal stromal cells represent the main source of bone formed by adult bone marrow. Cell Stem Cell *15*, 154–168.

Ziegler, A.N., Levison, S.W., and Wood, T.L. (2015). Insulin and IGF receptor signalling in neural-stem-cell homeostasis. Nat. Rev. Endocrinol. *11*, 161–170.

STAR★METHODS

KEY RESOURCES TABLE

REAGENT or RESOURCE	SOURCE	IDENTIFIER
Antibodies		
total AKT	Cell Signaling Technology	9272; RRID: AB_329827
pSer473AKT	Cell Signaling Technology	4051; RRID: AB_331158
total ERK2	Santacruz	sc-154; RRID: AB_2141292
pERK1/2	Santacruz	sc-7383; RRID: AB_627545
total JAK2	Cell Signaling Technology	3230S; RRID: AB_2128522
pJAK2	Cell Signaling Technology	3771S; RRID: AB_330403
total STAT3	Cell Signaling Technology	12640s; RRID: AB_2629499
pSTAT3	Cell Signaling Technology	9145S; RRID: AB_2491009
β-Actin	Sigma-Aldrich	A2066; RRID: AB_476693
List of FACS antibodies, see Table S5	This paper	N/A
digoxigenin (DIG)-labeled tyramide	PerkinElmer	NEL748001KT
alkaline-phosphatase-conjugated sheep anti-DIG FAB-fragments	Roche	11093274910; RRID: AB_514497
Chemicals, Peptides, and Recombinant Proteins		
S961 (insulin receptor antagonist)	www.antibodies-online.com	ABIN2876379
Human Leptin	Sigma	L-4146
Human Insulin	Sigma	I2643
Critical Commercial Assays		
Human Adiponectin ELISA kit	ALPCO	80-ADPHU-E01
Human Leptin ELISA kit	R&D Biosystems	DLP00
Human P1NP ELISA kit	Roche Diagnostics	03141071 190
Human CTX ELISA kit	Roche Diagnostics	11972308 122
Human MicroVue TRAP5b Assay	Quidel	8036 (XUS)
U-plex: IL-1α; IL-1RA, MCP-1, SDF-1α	MesoScale	K15067-1
V-plex IL-1β, IL-4, IL-6, IL-8, IL-10, TNF-α	MesoScale	K151A9H-1
pSer473-AKT kit	MesoScale	K150MND
Total AKT kit	MesoScale	K150MOD
β-galactosidase staining	Cell Signaling	9860
SA-β-gal Activity 96-well assay kit	Cell Biolabs	CBA-231
Cellular Reactive Oxygen Species (ROS) Detection assay	Abcam	ab113851
Seahorse XF Cell Mito Stress Test Kit	Agilent	103015-100
TruSeq Illumina mRNA prep kit	Illumina	RS-122-2001
HiSeq v4 Illumina SR sequencing kit	Illumina	GD-401-4001 FC-401-4002
Deposited Data		
Analyzed RNaseq data, see Table S3	This paper	N/A
Experimental Models: Cell Lines		
Human: immortalized bone marrow skeletal stem cells hBM-MSC	Abdallah et al., 2005	N/A
Oligonucleotides		
List of primers, see Table S6	This paper	N/A
siRNA targeting sequence: INSR: GCAUCGAGAAGAACAAUGAtt	Ambion	s533803
siRNA targeting sequence: LEPR: GAAUACUUCAAAUUCGAAUtt	Ambion	s8137
In situ hybridization probe against LepR mRNA	ACD Bioscience	410381
In situ hybridization probe against InsR mRNA	ACD Bioscience	450061

(*Continued on next page*)

Continued

REAGENT or RESOURCE	SOURCE	IDENTIFIER
Software and Algorithms		
Kaluza 1.1	Beckman Coulter	https://www.beckman.com/flow-cytometry/software/kaluza
Image Lab	BioRad	http://www.bio-rad.com/en-dk/product/image-lab-software?ID=KRE6P5E8Z
GraphPad Prism 5.0a	GraphPad	https://www.graphpad.com/support/prism-5-updates/

CONTACT FOR REAGENT AND RESOURCE SHARING

Further information and requests for resources and reagents should be directed to and will be fulfilled by the Lead Contact, Michaela Tencerova, PhD (mtencerova@health.sdu.dk).

EXPERIMENTAL MODEL AND SUBJECT DETAILS

Human subjects

Participants including lean (n = 19), overweight (n = 15) and obese (n = 20) healthy men (age 33 ± 2 years; body mass index (BMI) 21-41 kg/m^2) were recruited from the local community. Exclusion criteria were known metabolic bone disease, known diabetes mellitus and use of medication or concomitant diseases that influence bone and fat metabolism such as glucocorticoids and anabolic drugs as well as impaired renal and hepatic function. The study was performed according to the Declaration of Helsinki and was approved by the Regional Committees on Health Research Ethics for Southern Denmark (Project-ID: S-20150013). All participants signed informed consent prior to participation in the study.

Isolation and culture of bone marrow stromal stem cells from bone marrow aspirates

Bone marrow samples were obtained by aspiration of 10-15mL from the iliac crest after infiltration of the area with local anesthetic (lidocaine, 10 mg/mL), in a 20-mL syringe and mixed 1:1 with heparin (100 U/mL). Low-density mononuclear cells were isolated through centrifugation with a Lymphoprep density gradient (density = 1.077 ± 0.001 g/cm^2) and then selected through the process of plastic adherence. Cells were then cultured at 1x10^5 cells/cm^2 (1x10^6 cells per chamber slide) in Minimal Essential Media (MEM) containing 10% fetal bovine serum (FBS, GIBCO) incubated at 5% CO_2 at 37°C and then nourished by completely changing the medium once a week along with passage at 70% confluence. Cultured cells were sub-cultured and further studied in differentiation conditions to induce adipogenesis and osteogenesis, respectively.

Isolation and culture of adipose-derived stromal cells (AT-MSCs) from needle biopsy

A needle biopsy (size 12G) from the subcutaneous abdominal adipose tissue was obtained after the OGTT to isolate adipose-derived MSC (AT-MSCs). AT-MSCs were isolated according to a previous publication (slightly modified) (Rossmeislová et al., 2013) following digestions with Collagenase I (200 U/mL), centrifugation steps, red blood cells (RBC) lysis and washing steps with PBS. Initially, the cells were plated in culture dishes in DMEM/F12 culture medium with 10% fetal bovine serum (FBS), incubated at 5% CO_2 at 37°C and then nourished by completely changing the medium once every three days along with a passage at 80% confluence. After expansion *in vitro* the cells were sub-cultured and further studied in differentiation conditions to induce adipogenesis.

METHOD DETAILS

Clinical investigations

Bone mass, body composition and metabolic characteristics were analyzed using DXA scan, oral glucose tolerance test (OGTT) and standard biochemical analysis.

Oral glucose tolerance test (OGTT)

A 2 hour OGTT was performed with 75 g of glucose load. Venous blood was drawn from an antecubital vein at time 0, 30 and 120 min after the glucose administration to determine plasma glucose (ABL 800Flex, Radiometer, Denmark) and serum levels of insulin and C-peptide (Cobas e411 analyzer, Roche Diagnostics, Denmark). The OGTT was performed after an overnight fast of at least ten hours. Additionally, fasting venous blood was collected for subsequent biochemical analyses and stored at −80°C. HOMA-IR (homeostasis model assessment of the insulin resistance index) was calculated as follows: (fasting insulin (mU/L)_fasting glucose (mmol/L))/22.5.

DXA scans

Total lean and total fat mass were measured by DXA (Hologic Discovery, Waltham, Massachusetts, USA), and these data were used to calculate fat distribution. Areal bone mineral density (aBMD) was measured at the lumbar spine (L1-L4), total hip and the femoral neck using DXA.

Biochemical analyses

Biochemical analyses (hormone and lipid profiles) were performed by the hospital laboratory in blood samples drawn in fasting state. Serum levels of adiponectin and leptin were measured by ELISA kit (ALPCO and R&D Biosystems, respectively). Measurement of fasting serum procollagen type I amino-terminal propeptide (P1NP) (CV 10%, LOD 5 ng/mL) and C-telopeptide of type I collagen (CTX) were both performed by validated routine methods (Cobas e602 analyzer, Roche Diagnostics, Denmark), the limit of detection (LOD) for P1NP and CTX were 5ng/mL and 0.01 ng/mL, respectively, and the interassay coefficients of variation (CV) on two levels for both methods were 10% or lower. Levels of tartrate-resistant acid phosphatase 5b (Trap5b) were measured by a commercially available immunocapture enzyme assay (MicroVue TRAP5b, Quidel, San Diego, USA) according to the manufacturer's protocol (CV 10%, LOD 0.2 U/L). Quantitative analysis of inflammatory cytokines/chemokines (U-plex: IL-1α; IL-1RA, MCP-1, SDF-1α and V-plex IL-1β, IL-4, IL-6, IL-8, IL-10, TNF-α) in plasma samples was performed using Immunoplex kits (MesoScale) and a MESO QuickPlex machine (MesoScaleDiscovery).

Flow cytometry

BM-MSC were immunophenotyped using a panel of MSC cell markers (see the list in Table S5). Adherent cells were removed from flasks using 0.05% trypsin EDTA, incubated with Fc-blocking solution followed by incubation with pre-conjugated antibodies according to manufacturer recommendations. The flow cytometry was performed by BD LSR II (BD Biosciences) and analyzed by Kaluza 1.1 analysis software.

For the cell sorting experiments, hBM-MSCs were incubated with Fc-blocking solution followed by incubation with pre-conjugated antibodies either LEPR-PE (Miltenyi) or IR- PE antibody (BD Bioscience) and were run through a BD FACS Aria III (BD Bioscience). Representative gating scheme is shown in Figures S3A and S3B. LEPR+/− and IR+/− subpopulations were collected and sub-cultured *in vitro* for subsequent cellular analyses.

Cells proliferation

Primary BM-MSCs were plated in 6-well plates at a density of 10,000 cells/well in a standard growth medium supplemented with 10% FBS. Cells number was evaluated every day from 1 to 14. Cells were washed with PBS, harvested by trypsinization and manually counted in triplicate using Burker-Turk counting chambers.

Colony forming unit-fibroblast (CFU-f) assay

For assessment of CFU, cells were plated in p0 at a density of 0.5 million and 1 million cells in T75 flask. After 14 days, colonies displaying more than 50 cells were counted using Crystal Violet staining (Sigma-Aldrich).

In vitro differentiation

Adipocyte differentiation

Cells were plated at a density of 30000 cells/cm^2. Adipocytic induction media DMEM, containing 10% FBS, 10% Horse serum (GIBCO), 100 U/mL penicillin (GIBCO), 100 μg/mL streptomycin (GIBCO), 100 nM dexamethasone (Sigma-Aldrich), 0.25 mM 3-isobutyl-1-methyxanthine (IBMX), 1 μM BRL (Sigma-Aldrich), 3 μg/mL Insulin (Sigma-Aldrich), was changed every other day for 10 days.

Oil Red O staining

At day 10 of adipocyte differentiation, cells were fixed in 4% paraformaldehyde for 10 min at room temperature then stained with Oil Red O (Sigma-Aldrich) to visualize the lipid content. Briefly, cells were rinsed in 3% isopropanol solution and stained with filtered Oil Red O solution (0.5 g in 100% isopropanol) for 1 h at room temperature (RT).

Osteoblast differentiation

The cells were plated at a density of 20000 cells/cm^2 in alpha MEM medium (GIBCO) containing 10% FBS, 100 U/mL penicillin (GIBCO), 100 μg/mL streptomycin (GIBCO). Osteoblast induction media was composed of base medium supplemented with 10 mM B-glycerophosphate (Sigma-Aldrich), 10 nM dexamethasone (Sigma-Aldrich), 50 μg/mL Vitamin C (Sigma-Aldrich) and 50 μg/mL Vitamin D (Sigma-Aldrich) replaced media one day after the seeding. The medium was changed every other day for 10 days.

Alizarin Red staining

Mineralized matrix formation at day 10 of osteoblast differentiation, was measured using Alizarin red staining (Abdallah et al., 2006). Cells were fixed with 70% ice-cold ethanol for 1 h at −20°C before addition of AR-S (40 mM; Sigma-Aldrich) dissolved in distilled

water (pH 4.2). The cells were stained for 10 min at RT. The level of calcium deposition was quantified by elution of AR-S following incubation in 10% cetylpyridinium chloride (Sigma-Aldrich) for 1 h at RT. The absorbance of the eluted dye was assessed at 570 nm in a FLU Ostar®Omega plate reader.

Alkaline phosphatase (ALP) activity assay

Cells were incubated with naphthol AS-TR phosphate solution containing Fast Red TR (Sigma-Aldrich) as described previously (Abdallah et al., 2006). Alkaline phosphatase activity was measured using p-nitrophenyl phosphate (Fluka Chemie) as substrate (Qiu et al., 2007).

Insulin responsiveness of BM-MSCs and AT-MSCs

Undifferentiated and AD differentiated cells were starved overnight in serum free media. The following day the cells were stimulated with 100nM insulin (Sigma Aldrich) for 15 min and then harvested for protein used in subsequent analyses.

Senescence-associated β-galactosidase (β-gal) activity assay

SA-β-gal Activity 96-well assay kit was used (Cell Biolabs, Inc-USA, Catalog Number CBA-231) to determine the cellular senescence by measuring SA-β-Gal activity using a fluorometric substrate according to the manufacture protocol. All reagents were prepared fresh on the day of the assay. Cells were seeded at density $1.5x10^4$ cells /well in black 96-well plate clear bottom. Following day viability dye was added (10%) to the culture media and incubated in the dark at 37°C for 1h. Measurement was subsequently taken using fluorescent mode (Ex 530 nm/Em 590 nm). The results were normalized to the number of cells/well and expressed as % SA-β-gal activity.

Senescence-associated β-galactosidase Staining

To examine the senescence in the cells we used a commercial kit for β-galactosidase staining (Cell Signaling Technology-Netherlands, Cat# 9860). Cells were cultured in black 96-well plate clear bottom at 1.5 $x10^4$ cells /well 24 hours before the assay. Media were removed and cells were washed with PBS, and then fixed for 10 minutes at room temperature. After fixation the cells were rinsed with PBS and incubated with β-galactosidase staining solution (pH = 6.0) at 37°C in dry incubator (no CO_2) overnight. The blue color as a reaction results was monitored after 12h. Images of cells were taken with inverted microscope under bright field.

Cellular Reactive Oxygen Species (ROS) Detection assay

DCFDA (2,7-dichloro-dihydro-fluorescein diacetate) (Abcam, Cambridge, MA) was used to measure the intracellular ROS levels. The cells were seeded at $2.5x10^4$ cells/well into a black 96 well plate with a clear bottom 24 hours before the assay. Culture media was replaced with DMEM complete culture media without phenol red supplemented with tert-butyl hydrogen peroxide (TBHP) at 100μM for 2 hours at 5.5% CO_2 incubator and 37°C. Media with TBHP was removed and cells were loaded with DCFDA 25μM and incubated for 45 minutes at 37°C. DCFDA was removed and experimental conditions (media with or without TBHP) were added again to the cells. Then, the fluorescent intensity was measured at Excitation 485 nm and Emission 535 nm kinetically using microplate reader every 1 minute for 30 minutes.

Mitochondrial stress test

IR ± and LEPR ± sorted cells and transfected hBM-MSCs were seeded at density 15 000 cells/ well in 8 multi-well plates (Agilent, Seahorse Bioscience) and analyzed in undifferentiated condition. Oxygen consumption rate (OCR) of non-differentiated cells were determined using an XFp Extracellular Flux Analyzer (Seahorse Bioscience) applying Mito stress test in XF media (non-buffered DMEM containing 10 mM glucose, 4 mM L-glutamine, and 2 mM sodium pyruvate) under basal conditions and in response to oligomycin (1 μM), 2 μM fluoro-carbonyl cyanide phenylhydrazone (FCCP) and 0.5 μM rotenone + 0.5 μM antimycin A. Basal OCR was calculated by subtraction of rotenone- and antimycin A-induced OCR (1 μM of each inhibitor) to the unstimulated OCR value. Maximal respiration was determined using FCCP (2 μM) according to Wu et al. (2007). The data were analyzed using Wave Software (Seahorse Bioscience).

Treatment of BM-MSCs with S961 (insulin receptor antagonist)

hBM-MSCs were treated during AD differentiation with an insulin receptor antagonist at two different concentrations (10 or 100 nM) (S961; cat.n. ABIN2876379) (www.antibodies-online.com) for 10 days. The AD differentiated cells were harvested after 10 days for subsequent analyses.

siRNA transfection of hBM-MSCs

hBM-MSCs were transfected with the small interfering RNA (siRNA), targeting INSR (ID# s533803), LEPR (ID# s8137) as well as non-targeting siRNA (siRNA negative control, SCR cat# 4390846) were purchased from Ambion (Life Technology Inc). siRNA

were transfected to hBM-MSCs at a final concentration of 25 nM by Lipofectamine2000 (Invitrogen) as previously described (Chen et al., 2018) and according to the manufacturer's instructions. Transfection cocktail was subsequently replaced after 7 hours with normal culture media without antibiotics. 48 hours post transfection culture media was replaced with adipogenic or osteogenic differentiation media as described above.

Treatment of transfected and sorted hBM-MSCs with insulin and leptin

hBM-MSCs were transfected with INSR-siRNA or LEPR-siRNA and Scr-siRNA as a control, day 2 post transfection, the transfected cells and sorted cells were incubated in MEM/0.5% BSA media for 4 hours followed by insulin stimulation (100nM) for 15 minutes or (100nM) leptin stimulation (L-4146, Sigma) for 10 minutes. Then the cells were harvested for subsequent western blot analyses.

RNA extraction and Real time qRT-PCR

RNA was extracted using TRIzol then the QIAGEN Rneasy Mini Kit (QIAGEN) and reverse-transcribed using a RevertAid H Minus First Strand cDNA Synthesis Kit (Thermo Scientific). Quantitative real-time PCR was performed with an Applied Biosystems 7500 Real-Time PCR System using Fast SYBR Green Master Mix (Applied Biosystems) with specific primers (Table S6). β-actin was used as an endogenous control. Results are expressed as delta-delta Ct values.

RNA sequencing of BM-MSCs

RNA-seq was performed on RNA isolated from BM-MSC samples from lean and obese subjects (n = 10 per group). Unstranded, single read RNA-seq libraries were constructed from 1 μg total RNA using the NEBNext Ultra II procedure (New England Biolabs) and sequenced on the HiSeq 1500 platform (Illumina). Sequenced reads were mapped up against a human transcriptome index, and counted in annotated transcripts using the quasi-based mapping mode of Salmon (default parameters) (Patro et al., 2017). The transcriptome index was build using Ensembl genome version GRCh38 and Gencode v24 annotations (both files obtained from encodeproject.org).

The differential expression analysis was done on raw RNA-seq counts by the DESeq2 method (Love et al., 2014) comparing obese to lean. Genes with a false discovery rate (FDR) below 0.1 were considered as differentially expressed.

Gene ontology (GO) enrichment was done by comparing the frequency of genes from a GO category in the differentially regulated gene sets, to the frequency in the whole dataset using fisher exact tests. Shown GO categories are selected from a longer list of significantly enriched GO-categories ($p < 0.05$), and are displayed as how frequent genes of the GO category are found in the differentially expressed gene sets (%).

Western blot

Protein lysates were prepared using M2 lysis buffer including protease inhibitors. Protein concentration was measured using BCA assay (Thermo Scientific). Extracts (25 μg of protein) were examined by protein immunoblot analysis by probing with antibodies to total AKT (#9272, Cell Signaling), pSer473AKT (#4051, Cell Signaling), total ERK2 (#sc-154, Santacruz), (# pERK1/2 (#sc-7383, Santacruz), total JAK2 (#3230S, Cell Signaling), pJAK2 (#3771S, Cell Signaling), total STAT3 (#12640s, Cell Signaling), pSTAT3 (#9145S, Cell Signaling), β-Actin (A2066, Sigma-Aldrich). Immunocomplexes were detected by enhanced chemiluminescence and analyzed by Image Lab software (BioRad).

Multiplexed ELISA of Protein Phosphorylation

Quantitative analysis of pSer473-AKT/AKT in cell lysates of BMSC was performed using Immunoplex kits (MesoScale) and a MESO QuickPlex machine (MesoScaleDiscovery) (Gowan et al., 2007).

In situ *hybridization Analyses of Human Bone Specimens*

Formalin-fixed, decalcified and paraffin-embedded bone specimens from four human healthy volunteers (2 men and 2 women; aged 27-49 years, BMI 27-38 kg/m^2) were included *in situ* hybridization analysis. The biopsies were collected according to the Declaration of Helsinki and approval by the Regional Committees on Health Research Ethics for Southern Denmark (Projekt ID S-20110112). All participants signed informed consent prior to participation in the study. Paraffin sections (3.5-μm thick) were *in situ* hybridization using an enhanced version of the RNAScope 2.5 high definition procedure (310035, ACD Bioscience, Newark, CA, US). Sections were rehydrated, deparaffinized and pretreated as previously (Lassen et al., 2017), and hybridized overnight at 40°C with 20-ZZ-pair probes binding either human InsR mRNA (450061, ABD Bioscience) or LepR mRNA (410381, ACD Bioscience) diluted 1:1 in probe diluent (449819, ACD Bioscience). A negative control only hybridized with probe diluent was included. The amplification was conducted according to the instructions provided by the manufacturer. The horse radish peroxidase was further enhanced with digoxigenin (DIG)-labeled tyramide (NEL748001KT, PerkinElmer, Skovlunde, Denmark), which was labeled with alkaline-phosphatase-conjugated sheep anti-DIG FAB-fragments (11093274910, Roche, Hvidovre, Denmark) and visualized with Liquid Permanent Red (DAKO, Glostup, Denmark). Finally, the sections were counterstained with Mayer's Haematoxylin and mounted with Aqua-Mount.

QUANTIFICATION AND STATISTICAL ANALYSIS

Statistical analyses

The statistical significance of the differences in the means of experimental groups (lean, overweight and obese subjects) were determined by unpaired t test or analysis of variance (ANOVA) and Bonferroni or Tukey post hoc tests using GraphPad Prism 5.0a software. Data are presented as means ± SEM. P value < 0.05 was considered significant. All the statistical details of experiments can be found in the figure legends.

DATA AND SOFTWARE AVAILABILITY

Due to issues related to patient confidentiality, raw RNA seq data is not currently available for a public repository. If consent and approval are granted in the future, the raw data will be made available at that time. With specific questions related to data, please contact the lead contact.